universität wien

MASTERARBEIT / MASTER'S THESIS

Titel der Masterarbeit / Title of the Master's Thesis

„Characterising Strategies of Biochemical Regulation in Higher Plants: Patterns in the Diurnal Regulation of the Primary Metabolism in *Arabidopsis thaliana*"

verfasst von / submitted by

Jakob Weiszmann, BSc

angestrebter akademischer Grad / in partial fulfilment of the requirements for the degree of

Master of Science (MSc)

Wien, 2016 / Vienna 2016

Studienkennzahl lt. Studienblatt / degree programme code as it appears on the student record sheet:	A 066 832
Studienrichtung lt. Studienblatt / degree programme as it appears on the student record sheet:	Masterstudium Botanik
Betreut von / Supervisor:	Univ.-Prof. Dr. Wolfram Weckwerth

Table of Contents

1. Acknowledgements

Ich möchte mich an dieser Stelle bei all jenen bedanken, die mich im Laufe meines Studiums und insbesondere während der Entstehung dieser Arbeit begleitet und unterstützt haben.

Bedanken möchte ich mich bei Wolfram Weckwerth, der es mir möglich gemacht hat in seinem Department an diesem faszinierenden Projekt arbeiten zu dürfen und mir von Beginn an großes Vertrauen entgegengebracht hat.

Ganz besonders möchte ich Thomas Nägele dafür danken, dass er mich geduldig in das Thema der Modellierung eingeführt hat und mir als Betreuer stets für Fragen und Diskussionen – egal ob halb 9 im Büro oder halb zehn im SV - zur Verfügung stand.

Weiters möchte ich mich bei allen Kollegen aus dem MoSyS Department, nicht nur für die produktive und angenehme Zusammenarbeit bedanken, sondern auch dafür, dass ich von Anfang an herzlich aufgenommen wurde und Freunde finden konnte, die auch arbeitsunabhängig immer gerne treffe.

Insbesondere Lisa Fürtauer, die sich viel Zeit genommen hat um den Inhalt und die Formulierungen dieser Arbeit kritisch ∨ humorvoll zu bearbeiten und zu kommentieren.

I would also like to thank Lei Wang, not only for providing me with input for my thesis, but also for introducing me to my first words in Chinese (西红柿炒鸡蛋和米饭 谢谢).

A big thanks goes to Ella Nukarinen for providing the proteomics data.

Ein ganz spezieller Dank geht an meine Eltern, die mich immer unterstützt und motiviert haben. Insbesondere die montägliche Versorgung an hochwertigen Kohlehydraten hat es mir (und sicher auch meinen Kollegen) jedes Mal erlaubt energetisch in die Woche zu starten!

Auch meinen zwei Brüdern möchte ich dafür danken, dass sie immer für mich da waren.

Ein besonderer Dank für ihre sehr geschätzten und fachlich wertvollen Kommentare geht an Mia Miep.

Ich möchte mich auch bei Lisa dafür bedanken, dass sie immer und in allen Situationen meines Lebens an meiner Seite steht.

2. Abstract

In plants, diurnal regulation has been shown to be essentially involved in growth control, developmental processes and responses towards stress and fluctuating environmental conditions. Diurnal reprogramming of metabolism is required to cope with the broad range of external parameters faced by plants during the course of a day/night cycle. Yet, the derivation of conclusive hypotheses dealing with these regulatory strategies from experimental datasets is impeded by numerous regulatory circuits, non-linear enzyme kinetics and thermodynamic constraints. To overcome this limitation and gain insight into the regulation of metabolism in *Arabidopsis thaliana*, a covariance-based steady-state modelling approach was applied for the functional integration of metabolomics data. The inverse approximation of biochemical Jacobian matrices identified alpha- ketoglutarate, glutamate and glucose as key elements in diurnal regulation of primary metabolism. Additionally, diurnal dynamics in core enzymatic reactions could be characterized and validated by literature data and a proteomics dataset. Particularly, an increase of alpha- ketoglutarate dehydrogenase protein abundance and a peak in activity of two central transamination reactions could successfully be predicted. Finally, to facilitate the extraction of meaningful biochemical networks from genome scale reconstructions a user friendly graphical user interface (GUI) was developed.

3. Kurzfassung

In Pflanzen stellt die diurnale Regulation von Stoffwechselprozessen eine Voraussetzung für die effiziente Kontrolle von Wachstum, Entwicklungsprozessen und Stressreaktionen dar. Die tageszeitabhängige Anpassung des Stoffwechsels ist für Pflanzen nötig, um auf eine Vielfalt äußerer Parameter reagieren zu können. Jedoch stellt die Ableitung zugrundeliegender Regulationsmechanismen aus Experimentaldaten eine Herausforderung dar, da sich eine Vielzahl regulatorischer Kreisläufe nichtlinear verhält und daher eine intuitive Interpretation erschweren. In der vorliegenden Arbeit wurde daher eine auf experimenteller Kovarianzinformation basierende mathematische Methode angewandt, welche experimentell ermittelte Stoffwechseldynamiken mit einem biochemischen Netzwerk verknüpfte. Mit diesem Ansatz konnte gezeigt werden, dass die diurnale Regulation der Konzentrationen von alpha- Ketoglutarat, Glutamat und Glukose eine zentrale Rolle im pflanzlichen Primärstoffwechsel spielt. Darüber hinaus wurden Enzymreaktionen, die starken Einfluss auf die diurnale Dynamik des Primärstoffwechsels ausüben, identifiziert. Schließlich wurde eine computergestützte Benutzeroberfläche entwickelt, die die Reduktion von genombasierten, biochemischen Netzwerken auf experimentell validierbare Kernstrukturen erleichtert.

4. Introduction

4.1. Aim

This study aimed at the identification of biochemical key elements in the diurnal regulation of primary metabolism in the model plant *Arabidopsis thaliana* by the functional integration of large scale metabolomics data in metabolic network structures. A covariance based steady-state modelling approach was applied, potentially connecting experimental data with biochemical network information, which was extracted from published genome scale metabolic reconstructions. Finally, identified central metabolites and predictions of their influence on the regulation of key reactions were validated by the analysis of published gene expression studies and enzyme kinetics, as well as the interpretation of a proteomic data set. Additionally, a workflow for the efficient extraction of meaningful core networks from large metabolic networks was established to facilitate and speed up approaches requiring information about the biochemical connections of a specific set of metabolites.

First, representing a central part of metabolism in plants, a concise model of the tricarboxylic acid cycle was examined. Though, from a physiological point of view it is a small part in a vast regulatory network, therefore a larger model, which additionally incorporated numerous reactions of the main carbohydrate and amino acid pathways was constructed. This allowed the examination of regulation patterns and the identification of key metabolites throughout a broad part of the plants primary metabolism.

4.2. The genetic model plant *Arabidopsis thaliana*

Arabidopsis thaliana is a member of the Brassicaceae family and probably the best characterized plant on a molecular genetic level. It is an annual ruderal plant with a life cycle duration of 10-12 weeks in its natural habitat, which can be shortened to around 6 weeks in optimal, controlled conditions. Flowering is induced by long days and can be initiated earlier than usual by subjecting the plants to light period durations of ≥ 16 hours (Kadereit, Kost, & Sonnewald, 2014). There are numerous natural accessions colonizing a wide geographic range, from Europe, Asia and northern America to isolated occurrences in Australia and Africa (Hoffmann, 2002; Koornneef, Alonso-Blanco, & Vreugdenhil, 2004).

A. thaliana has been intensely studied as a model organism for the extension of knowledge about molecular, physiological, genetic and ecological aspects in plants since it was proposed

as an appropriate study object by Friedrich Laibach (Laibach, 1943). In modern studies it is still appreciated for the originally described traits of (I) high fertility, (II) easy cultivation in limited space, (III) fast development, (IV) availability of many natural accessions, (V) easy crossing with a good fertility of hybrids, and (VI) a low chromosome number. Additionally the availability of seeds through seed stock facilities offering mutant lines and genetically distinct natural accessions makes experiments reproducible and convenient. It was chosen for this study because there is a broad base of biochemical knowledge readily available, which is imperative for the process of metabolic modelling. Further, there are vast datasets of published enzyme activity assays, transcriptomics and proteomics data sets, finally permitting a comprehensive validation of results and hypotheses acquired by modelling approaches.

4.3. Diurnal dynamics of metabolism in *Arabidopsis*

In many higher plants, e.g. in *A. thaliana*, numerous molecular processes are regulated depending on the phase of the day. Many of these processes are regulated by the circadian clock which represents an endogenous molecular oscillator and supposedly grant a remarkable evolutionary benefit (Dodd et al., 2005). Clock-regulated processes show a characteristic oscillating pattern, observable even if the organism is kept under constant light or darkness. Already centuries ago it was discovered that plants undergo rhythms, which are independent of illumination. According to Mancuso and colleagues the first notion of such movements, sustained even when the plant is kept in continuous darkness, was written down as early as 1729 (Mairan, 1729; Mancuso & Shabala, 2007). More recently, it has been shown on RNA level, that about one third of expressed genes in *Arabidopsis* are regulated by circadian clock mechanisms (Covington, Maloof, Straume, Kay, & Harmer, 2008). Blaesing and co-workers investigated diurnal gene expression patterns and found that both sugar availability and circadian clock mechanisms are major inputs of regulation (Blaesing et al., 2005). Harmer gave a detailed review of circadian clock regulation in plants (Harmer, 2009). In addition to processes regulated by the clock, there are many examples of plant responses to illumination and darkness, which do not continue to show their typical dynamics if the day-night cycle is interrupted or stopped. Diurnal rhythms affect almost all processes in plants and can be clearly observed in studies of metabolism when plants are sampled over the course of one or several dark-light periods. One prominent example in *Arabidopsis* is the dynamic accumulation of transitory leaf starch in the light period and its degradation in the dark providing the plant with sufficient energy and carbon equivalents (reviewed by Zeeman, Smith, and Smith 2004).

One described strategy of *Arabidopsis* growing in short day conditions is the up-regulation of transitory starch production, to supply sufficient carbon equivalents during the night, by activation of ADP-glucose pyrophosphorylase (Gibon, Blaesing, Palacios-Rojas, et al., 2004). In addition it was observed, that the plant adapts the rate of starch degradation during the dark phase in such a way, that the starch pool is continuously decreasing during the night, regulated by the length of the dark phase to counteract depletion of the sucrose pool before the next light period starts (Sulpice et al., 2014).

4.4. Metabolic Modelling in Systems Biology

Systems biology has become a rapidly growing research field and aims for the understanding of an organism not just as a sum of all analysed parts, but as a complex, interconnected and tightly regulated system. Frequently, approaches focus the iterative combination of experimental and computational methods.

Commonly, systems biology approaches aim at the identification and prediction of (molecular) phenotypes by the functional integration of experimental high throughput data applying various mathematical approaches (Weckwerth, 2011). Frequently, functional integration approaches result in multidimensional problems, which need computational strategies to enable the realistic interpretation of complex interactions between various levels of molecular organization. Hence, computationally assisted metabolic modelling approaches strive to depict available information about biochemical interactions of substances in a living organism as a mathematical representation (Steuer, 2007).

In the field of molecular systems biology, strategies of mathematical modeling have successfully been applied to approach various open research questions (for further information see (Töpfer, Kleessen, & Nikoloski, 2015; Watson, Yilmaz, & Walhout, 2015)). Flux Balance Analysis (FBA) is one of the most basic approaches calculating flux distributions in an organism at a hypothetical steady state. Such a steady state approach is based on the assumption that interconversions between metabolite pools are much faster than cell growth or environmental fluctuations. The optimisation of flux rates in FBA always relies on one predefined cost function, e.g. optimization of cellular growth or maximal generation of a desired product. Hence, it is much easier to apply this technique to single cell organisms than to differentiated multicellular organisms. All other constraints are given by the stoichiometry of the contained reactions and set upper and lower boundaries in which the reaction velocities

are allowed to fluctuate. This strategy is commonly used for the optimisation of industrial processes for the production of chemicals (see e.g. (Hsu & Lo, 2003)) or therapeutic substances, e.g. biopharmaceutical proteins (see e.g. (Meadows, Karnik, Lam, Forestell, & Snedecor, 2010)).

For the detailed and functional analysis of dynamics in a molecular system, kinetic modelling approaches have been shown to be suitable due to the functional analysis of reaction rates, which makes it possible to unravel specific functional properties. Examples for such kinetic approaches are studies on the discrimination of various cancer cell lines by identification of impaired molecular interactions (Mani et al., 2008) or the determination of diurnal dynamics of kinetic parameters belonging to the central carbohydrate metabolism in *Arabidopsis thaliana* (Nägele et al., 2010). The latter study allowed the estimation of the effect of a reduced activity of a vacuolar invertase on the diurnal regulation of carbon allocation on a whole-plant level. Nevertheless the construction of such kinetic models requires detailed knowledge about enzyme kinetic parameters and, is therefore limited to relatively small networks of well-studied organisms.

4.5. Ordinary differential equations and inverse approximation

Reactions in metabolic networks can be described as systems of ordinary differential equations (ODEs) in which changes of metabolite concentrations are described over changes in time (Equation 1).

$$\frac{dM}{dt} = \boldsymbol{N} * \boldsymbol{v} = f_M(t) \qquad \text{(Equation 1)}$$

Here, *M* is the concentration of a metabolite, ***v*** is a vector containing reaction rates and ***N*** represents the stoichiometric matrix of a metabolic system (Schallau & Junker, 2010). The stoichiometric matrix ***N*** has the dimensions s x m, where s is the number of species and m the number of reactions. It summarizes which metabolite takes part in which reactions. The entries of ***N,*** called stoichiometric coefficients, contain information about the consumption or production of the corresponding metabolites, denoted by positive, negative or zero entries. The term ***N*v*** represents all reactions contributing to the metabolic function of the metabolite of interest, such as its rate of biosynthesis, rate of degradation or the rate of transport. The vector ***v*** comprises reaction rates which are influenced by a vast number of parameters (**p**). For example, these parameters comprise protein levels and thermodynamic constraints. Due

to the large number and the multitude of dependencies between these parameters it is hardly possible to completely assess them experimentally. Even if enzyme kinetic parameters are available, e.g. from databases like BRENDA (http://www.brenda-enzymes.org/), they are frequently derived from *in vitro* studies under optimal conditions and can differ severely from the parameters prevalent *in vivo* (Minton, 2001; Teusink et al., 2000).

Yet, if sufficient parameters of the metabolite function were available it would be possible to numerically integrate the ODE systems enabling the simulation of time courses of metabolite concentrations. However, as it was illustrated before, the availability of parameters with adequate confidence is limited and parameter estimation techniques may introduce and amplify uncertainties (Gutenkunst et al., 2007; Schaber, Liebermeister, & Klipp, 2009).

To circumvent the limitation of large-scale metabolic models by (enzyme) kinetic parameters, Nägele and colleagues derived a strategy to directly infer Jacobian matrices from experimental covariance information of a metabolic steady state (Nägele et al., 2014). This strategy is based on the linearization of the nonlinear metabolic functions $f_{\mathbf{M}}(t)$ at a steady state and the partial differentiation of the functions with respect to metabolite concentrations, finally resulting in the Jacobian matrix **J**. (Equation 2)

$$\boldsymbol{J} = \begin{pmatrix} \frac{\partial f_1(\boldsymbol{M},\boldsymbol{p},t)}{\partial M_1} & \frac{\partial f_1(\boldsymbol{M},\boldsymbol{p},t)}{\partial M_2} & \cdots & \frac{\partial f_1(\boldsymbol{M},\boldsymbol{p},t)}{\partial M_n} \\ \frac{\partial f_2(\boldsymbol{M},\boldsymbol{p},t)}{\partial M_1} & \frac{\partial f_2(\boldsymbol{M},\boldsymbol{p},t)}{\partial M_2} & \cdots & \frac{\partial f_2(\boldsymbol{M},\boldsymbol{p},t)}{\partial M_n} \\ \vdots & \vdots & \ddots & \vdots \\ \frac{\partial f_n(\boldsymbol{M},\boldsymbol{p},t)}{\partial M_1} & \frac{\partial f_n(\boldsymbol{M},\boldsymbol{p},t)}{\partial M_2} & \cdots & \frac{\partial f_n(\boldsymbol{M},\boldsymbol{p},t)}{\partial M_n} \end{pmatrix} \qquad \text{(Equation 2)}$$

The direct inference of ***J*** from the covariance matrix ***C*** (Equation 3) is based on previous studies in which the theoretical basics (Van Kampen, 1992) as well as the biochemical interpretation were derived and explained (Nägele & Weckwerth, 2013; Steuer, Kurths, Fiehn, & Weckwerth, 2003; Sun & Weckwerth, 2012). The fluctuation matrix ***D*** on the right side of the equation introduces randomly generated noise to account for metabolite fluctuations.

$$\boldsymbol{JC} + \boldsymbol{CJ}^T = -2\boldsymbol{D} \qquad \text{(Equation 3)}$$

The covariances, which provide information about how two entities change together in a system, were calculated as shown in (Equation 4).

$$\mathrm{cov}(x_j, x_k) = \frac{1}{n-1}\sum_{i=1}^{n}(x_{ij} - \bar{x}_j)(x_{ik} - \bar{x}_k) \qquad \text{(Equation 4)}$$

Respectively the covariance matrices (***C***) incorporating all metabolites in the system were constructed in the manner:

$$\boldsymbol{C} = \begin{pmatrix} \frac{1}{n-1}\sum_{i=1}^{n}(x_{i1} - \bar{x}_1)(x_{i1} - \bar{x}_1) & \frac{1}{n-1}\sum_{i=1}^{n}(x_{i1} - \bar{x}_1)(x_{i2} - \bar{x}_2) & \cdots & \frac{1}{n-1}\sum_{i=1}^{n}(x_{i1} - \bar{x}_1)(x_{is} - \bar{x}_s) \\ \frac{1}{n-1}\sum_{i=1}^{n}(x_{i2} - \bar{x}_2)(x_{i1} - \bar{x}_1) & \frac{1}{n-1}\sum_{i=1}^{n}(x_{i2} - \bar{x}_2)(x_{i2} - \bar{x}_2) & \cdots & \frac{1}{n-1}\sum_{i=1}^{n}(x_{i2} - \bar{x}_2)(x_{is} - \bar{x}_s) \\ \vdots & \vdots & \ddots & \vdots \\ \frac{1}{n-1}\sum_{i=1}^{n}(x_{is} - \bar{x}_s)(x_{i1} - \bar{x}_1) & \frac{1}{n-1}\sum_{i=1}^{n}(x_{is} - \bar{x}_s)(x_{i2} - \bar{x}_2) & \cdots & \frac{1}{n-1}\sum_{i=1}^{n}(x_{is} - \bar{x}_s)(x_{is} - \bar{x}_s) \end{pmatrix}$$

Entries of the biochemical Jacobian describe the influence of (infinitesimally) small changes in the concentration of a metabolite on a metabolite function at a metabolic steady state (Nägele, 2014).

The application of Equation 3 for functional integration of experimental high throughput data in biochemical network structures has already been applied in previous studies, e.g. to identify metabolic key regulators in the low energy response of *Arabidopsis* (Nägele et al., 2014).

The biochemical network structure required for a modelling approach can either be constructed manually, or be derived from genome scale metabolic network reconstructions which are freely available for numerous model organisms and cell types (e.g.: de Oliveira Dal'Molin et al. 2010; Ryu, Kim, and Lee 2015; Orth et al. 2011). Due to the widespread convention of using the open SBML (Systems Biology Markup Language) data format (Hucka et al., 2003) to describe and distribute mathematical models, the availability of models describing diverse biological systems is high. The public reference repository BioModels currently lists over 140,000 models of various organisms and cell types (Juty et al., 2015) and this number is continuously growing.

Nevertheless the direct integration of metabolite data acquired by a GC-MS (Gas chromatography coupled to mass spectrometry) approach in such structures is not feasible as not all species (metabolites) contained in the full reconstruction can be monitored. Therefore it is necessary to remove metabolites which were not measured from the model and create

conglomerate reactions of steps which could not be resolved (Nägele et al., 2014). A genome scale metabolic reconstruction contains a comprehensive set of reactions which are encoded in the DNA. An extensive overview of the metabolic reconstruction process was given by Thiele and Palsson (Thiele & Palsson, 2010). However this does not mean that all these reactions are physiologically important or active at the current, examined state of the organism. For example a reaction which is part of an anabolic pathway, directly driven by photosynthesis will be present in the metabolic reconstruction, but will play a negligible role in the metabolic fluxes of sink tissue. Due to this every reaction must be critically evaluated to create a high confidence network for the organism taking the current state as well as the sampled organs into account. Even though this is a time consuming and laborious task, the careful curation and validation of a network ensures that all results from the following modelling procedure can be interpreted in a biochemical and physiological meaningful context. Without detailed information about the biochemical interactions of metabolites in the organism the application of a covariance based modelling strategy is highly speculative and it would be substantially harder to draw conclusions from the results.

5. Methods

5.1. Software and Versions

Table 1 gives a detailed overview of the most important software and versions used in this project.

Table 1 Software versions used in this project

Software	Version	Weblink / Publication
MATLAB®	8.4 R2014b (64bit)	The MathWorks, Inc www.mathworks.com
Bioinformatics Toolbox™	4.5	
SimBiology®	5.1 [trial version]	
CellDesigner™	4.4.	www.celldesigner.org (Funahashi, Matsuoka, Jouraku, Kitano, & Kikuchi, 2006)

5.2. Metabolic Network Reduction

A genome scale metabolic reconstruction work of a juvenile *Arabidopsis thaliana* leaf (Mintz-Oron et al. 2012) was used for the construction of the metabolic network required for the modelling approach. For the reproducible and reliable reduction of such large networks to meaningful core networks containing only metabolites included in the experimental analysis, a workflow, aided by a graphical user interface (GUI), was developed in the numerical computing environment MATLAB®.

In the first step of the workflow, a metabolic network in the SBML format is loaded. The algorithm detects if the loaded model contains information about subcellular localisation of the compounds and provides the possibility to decide if this subdivision should be retained or ignored. If metabolite measurements were conducted without subcellular fractionation of the samples the latter option should be chosen as this will combine all compartments finally leading to a substantial simplification of the model. Any physiologically unfeasible reactions resulting from this automated combination of compartments will be removed in one of the

following steps. The network's stoichiometry is visualised to identify and automatically remove species not taking part in any reaction, which are frequently included in large-scale metabolic network reconstructions. After the successful import of the SBML model according to the user's input all metabolites and the stoichiometric matrix are read from the model and saved to the MATLAB workspace. The extraction of the stoichiometry information is conducted using inbuilt functions of SimBiology®. If this MATLAB app is not available the stoichiometric matrix can also be extracted from the SBML model by other, non-commercial software like COPASI (Hoops et al., 2006). This information is subsequently used to create a logical or Boolean square interaction matrix, which indicates all interactions between the contained metabolites, but disregards the stoichiometric coefficients, which provide information about the amount of molecules taking part in the reaction. Then a list of the metabolites (.xslx, .xsl or .csv format), representing the species of interest for the final and reduced model structure is loaded and the contained names are compared to the species names prevalent in the provided network. This is necessary because every chemical compound can be addressed by a multitude of names or nomenclature conventions, which generally poses a big problem of working with metabolic networks (Merlet et al., 2016). The result of this step is a table which allows the user to map the metabolites of interest to the corresponding species. Additionally, it is possible to allocate several species to one metabolite which can be used for example if the network discriminates isoforms which cannot be distinguished in the measurements. After this the interaction matrix and the full metabolite list of the network are reduced to the raw network and visualized using the *biograph()* command, which is part of the MATLAB Bioinformatics Toolbox™. To facilitate the manual curation of the generated core network, an interactive table is prompted which can be used to edit the interaction network finally producing a high confidence network. A manual curation in this way ensures that only biochemically and physiologically feasible reactions are enclosed in the final network.

Due to the technical limitations in quantifying phosphorylated compounds by the GC-MS method, the artificial pool of activated compounds (AC) was introduced in the model used in this study. It structurally summarizes activated and phosphorylated compounds and does not comprise any experimental information about concentration of these compounds.

The visualisation of SBML models was performed with CellDesigner™ Ver. 4.4 (Funahashi et al., 2006).

5.3. Ordinary differential equations and inverse approximation

The mathematical description of metabolic networks was based on systems of ordinary differential equations, ODEs, (see Equation 1). Based on the ODE structure, all metabolite interactions were described by a square interaction matrix, which was derived from the stoichiometric matrix.

Jacobian Matrices were calculated iteratively utilizing a covariance based inverse approach as shown in (Equation 3). The absolutely quantified metabolite data, used for the calculation of the covariances, were provided by Dr. Thomas Nägele (Department of Ecogenomics and Systems Biology, University of Vienna) and were acquired by harvesting leaves of *A. thaliana* at 5 time points in the course of one light period (16 h light / 8 h dark) and analysing them with GC-MS as described by Doerfler and co-workers (Doerfler et al., 2013). The light period started at 6 am and lasted until 10 pm, represented by the respective time point names 6:00 – 22:00 in the following graphs. The medians and the interquartile ranges of these iterative calculations were then used for further analyses. As the covariance based modelling approach contained no information about feedback or feedforward regulations, the influence of a negative sign is difficult to discuss. Therefore each of the Jacobian entries is considered regardless of its sign and the absolute value was interpreted.

All computational steps were performed in the numerical computing environment MATLAB®.

6. Results

6.1. High confidence networks derived from genome sequence information

The previously described workflow for the reduction of network structures (see chapter 5.2) was utilized for the extraction of a high confidence network from a genome scale reconstruction (Mintz-Oron et al., 2012) of *Arabidopsis thaliana* leaf metabolism which contained 2463 metabolites in 2769 reactions (**Figure 1**). Additionally, the model contained information about subcellular compartmentation.

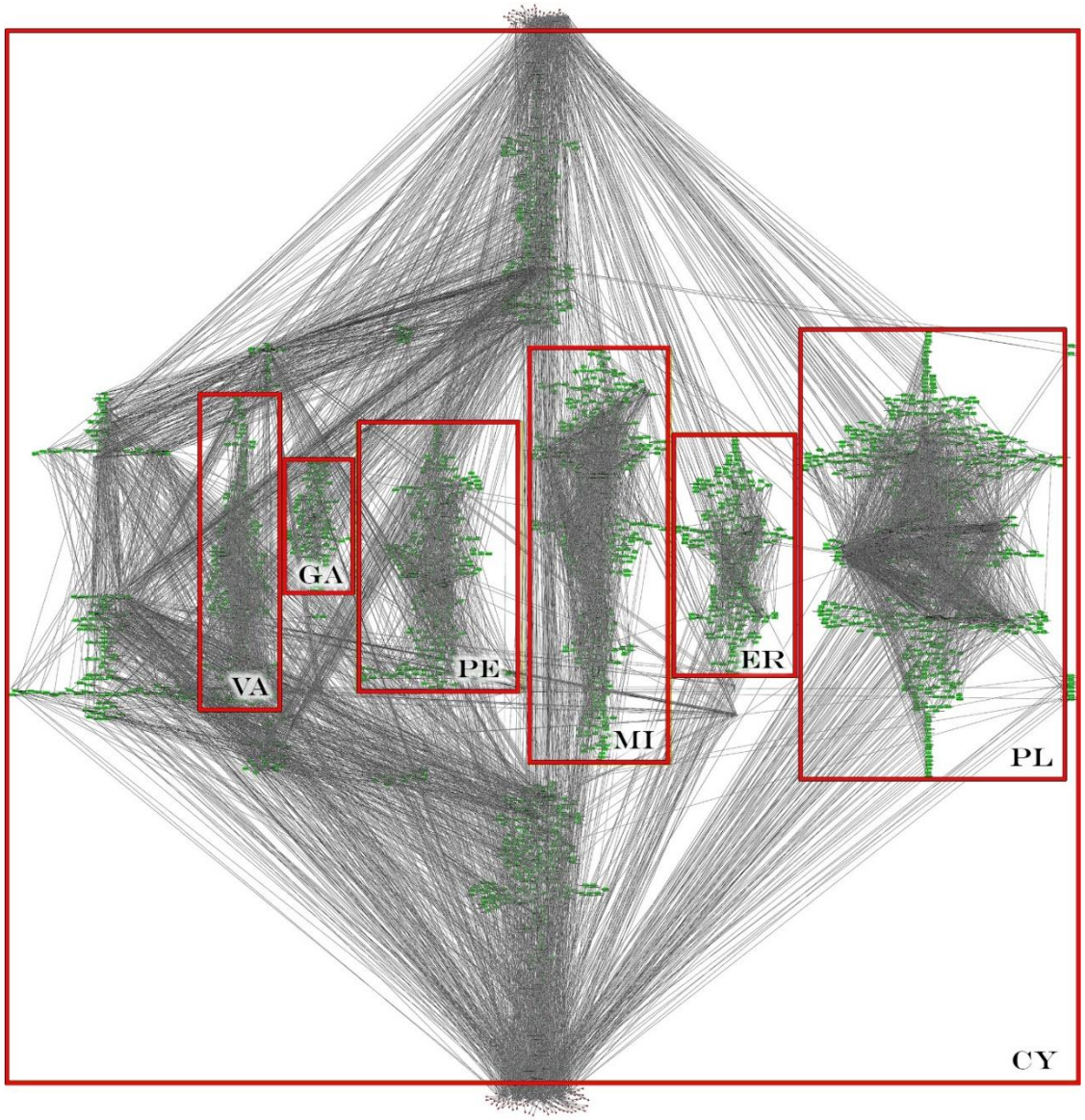

Figure 1 Graphical representation of the genome scale reconstruction of *Arabidopsis thaliana* leaf metabolism based on the SBML model published by Mintz-Oron and colleagues (Mintz-Oron et al.,

2012). Green boxes show metabolites, grey lines represent biochemical reactions and red squares indicate compartments. *VA* vacuole, *GA* golgi apparatus, *PE* peroxisome, *MI* mitochondrion, *ER* endoplasmic reticulum, *PL* plastid, *CY* cytosol.

The metabolic network, which resulted from the reduction process, comprised only the metabolites which were absolutely quantified in the GC-TOF/MS metabolomics experiment. Furthermore, it did not contain information about the subcellular localization of reactions and metabolites. Each reaction included in the final network was validated using a biochemical pathway database (www.biocyc.org)(Caspi et al., 2014) and literature data. A list of all reactions and participating enzymes identified by the corresponding enzyme commission (EC) numbers is provided in the Appendix, **Table S1**, and visualized in the high confidence network (**Figure 2**), which is referred to as model A in the following chapters.

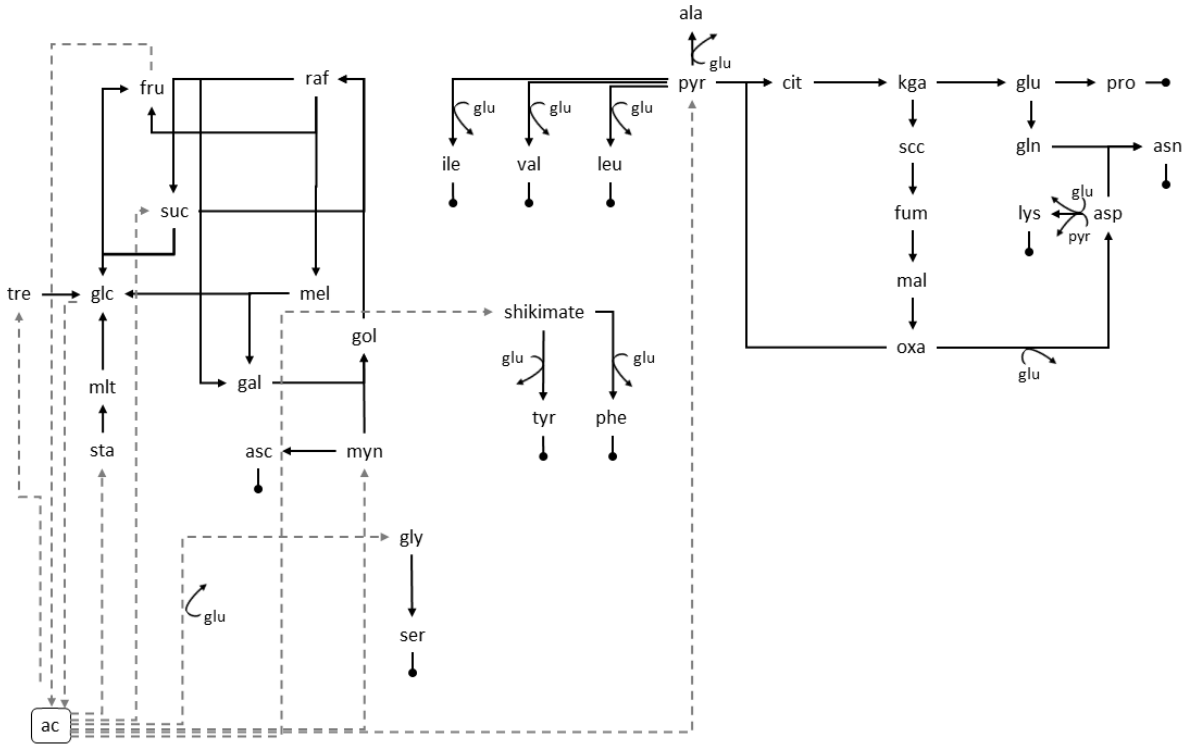

Figure 2 Schematic representation of the high confidence metabolic network. *ac* activated compounds, *tre* trehalose, *glc* glucose, *mlt* maltose, *suc* sucrose, *fru* fructose, *raf* raffinose, *mel* melibiose, *gal* galactose, *gol* galactinol, *myn* myo-inositol, *asc* ascorbate, *gly* glycine, *ser* serine, *ile* isoleucine, *val* valine, *leu* leucine, *pyr* pyruvate, *ala* alanine, *cit* citrate, *kga* alpha- ketoglutarate, *glu* glutamate, *pro* proline, *scc* succinate, *fum* fumarate, *mal* malate, *oxa* oxaloacetate, *asp* aspartate, *asn* asparagine, *gln* glutamine, *sta* starch.

6.2. Mathematical description of metabolic networks

The tricarboxylic acid (TCA) cycle (**Figure 3**) was mathematically described by a system of ordinary differential equations, ODEs (**Table 2**) and will be referred to as model B in the following chapters.

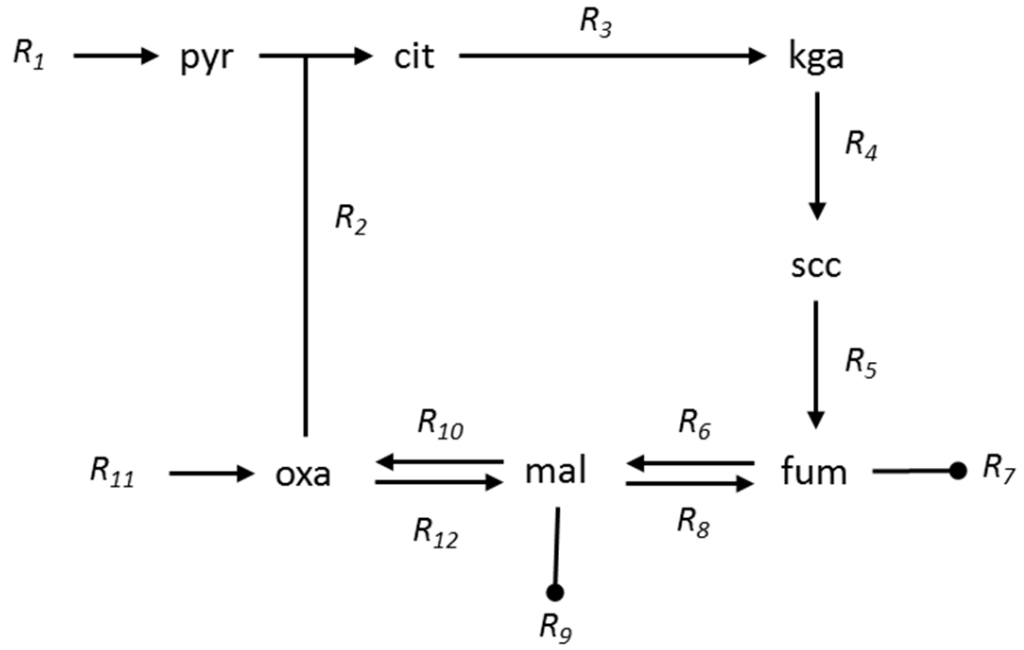

Figure 3 Simplified scheme of the TCA cycle. *pyr* pyruvate, c*it* citrate, *kga* alpha- ketoglutarate, s*cc* succinate, f*um* fumarate, m*al* malate, *oxa* oxaloacetate

This simple model comprised 7 metabolite pools, *S = {pyruvate, citrate, alpha- ketoglutarate, succinate, fumarate, malate, oxaloacetate}* and 12 biochemical reactions, $R = \{R_1, R_2, \ldots, R_{12}\}$. Each reaction *R* represented an enzymatic interconversion or transport reaction.

Table 2 Reactions in the TCA model and their representation as ODEs

Representation of reactions	ODEs
$R_1: \quad \varnothing \rightarrow pyruvate$	$\frac{d}{dt}(pyruvate) = R_1 - R_2$
$R_2: \quad pyruvate + oxaloacetate \rightarrow citrate$	$\frac{d}{dt}(citrate) = R_2 - R_3$
$R_3: \quad citrate \rightarrow alpha-ketoglutarate$	$\frac{d}{dt}(alpha\text{-}ketoglutarate) = R_3 - R_4$
$R_4: \quad alpha-ketoglutarate \rightarrow succinate$	$\frac{d}{dt}(succinate) = R_4 - R_5$
$R_5: \quad succinate \rightarrow fumarate$	$\frac{d}{dt}(fumarate) = R_5 + R_8 - R_6 - R_7$
$R_6: \quad fumarate \rightarrow malate$	$\frac{d}{dt}(malate) = R_6 + R_{12} - R_8 - R_9 - R_{10}$
$R_7: \quad fumarate \rightarrow \varnothing$	$\frac{d}{dt}(oxaloacetate) = R_{10} + R_{11} - R_{12} - R_2$
$R_8: \quad malate \rightarrow fumarate$	
$R_9: \quad malate \rightarrow \varnothing$	
$R_{10}: \quad malate \rightarrow oxaloacetate$	
$R_{11}: \quad \varnothing \rightarrow oxaloactate$	
$R_{12} \quad oxaloacetate \rightarrow malate$	
Where $\varnothing$ depicts an external space	

The ODE system was represented in form of the stoichiometric matrix ***N***.

$$\boldsymbol{N} = \begin{array}{c} \\ pyruvate \\ citrate \\ alpha-ketoglutarate \\ succinate \\ fumarate \\ malate \\ oxaloacetate \end{array} \begin{pmatrix} 1 & -1 & 0 & 0 & 0 & 0 & 0 & 0 & 0 & 0 & 0 & 0 \\ 0 & 1 & -1 & 0 & 0 & 0 & 0 & 0 & 0 & 0 & 0 & 0 \\ 0 & 0 & 1 & -1 & 0 & 0 & 0 & 0 & 0 & 0 & 0 & 0 \\ 0 & 0 & 0 & 1 & -1 & 0 & 0 & 0 & 0 & 0 & 0 & 0 \\ 0 & 0 & 0 & 0 & 1 & -1 & -1 & 1 & 0 & 0 & 0 & 0 \\ 0 & 0 & 0 & 0 & 0 & 1 & 0 & -1 & -1 & -1 & 0 & 1 \\ 0 & -1 & 0 & 0 & 0 & 0 & 0 & 0 & 0 & 1 & 1 & -1 \end{pmatrix}$$

A square interaction matrix ***I*** was derived indicating whether two metabolites biochemically interact (entry: 1) or not (entry: 0). This interaction matrix was applied for the inverse calculation of the Jacobian matrices.

$$\boldsymbol{I} = \begin{array}{c} \\ pyr \\ cit \\ kga \\ scc \\ fum \\ mal \\ oxa \end{array} \begin{array}{c} \begin{array}{ccccccc} pyr & cit & kga & scc & fum & mal & oxa \end{array} \\ \begin{pmatrix} 1 & 1 & 0 & 0 & 0 & 0 & 1 \\ 0 & 1 & 1 & 0 & 0 & 0 & 0 \\ 0 & 0 & 1 & 1 & 0 & 0 & 0 \\ 0 & 0 & 0 & 1 & 1 & 0 & 0 \\ 0 & 0 & 0 & 0 & 1 & 1 & 0 \\ 0 & 0 & 0 & 0 & 1 & 1 & 1 \\ 1 & 1 & 0 & 0 & 0 & 1 & 1 \end{pmatrix} \end{array}$$

The same procedure to describe metabolic networks by the generation of a system of ODEs was used for the high confidence network generated by the reduction strategy described in the previous chapter (chapter 5.2). The resulting interaction matrix is provided in the Appendix (**Table S4**).

6.3. Modelling the tricarboxylic acid cycle

To determine the number of replications which were, at least, necessary for a stable and reproducible inverse approximation of Jacobian matrices, 10^2, 10^3, $5*10^3$, 10^4 and 10^6 calculations were performed. The interquartile distances, which were determined by subtracting the 25 % quantile from the 75 % quantile, were analysed to indicate a stable technical variance of the calculations. Interquartile distances were found to be stable after $5*10^3$ calculations, (**Figure 4**), and, hence, all following calculations were conducted with $5*10^3$ repetitions.

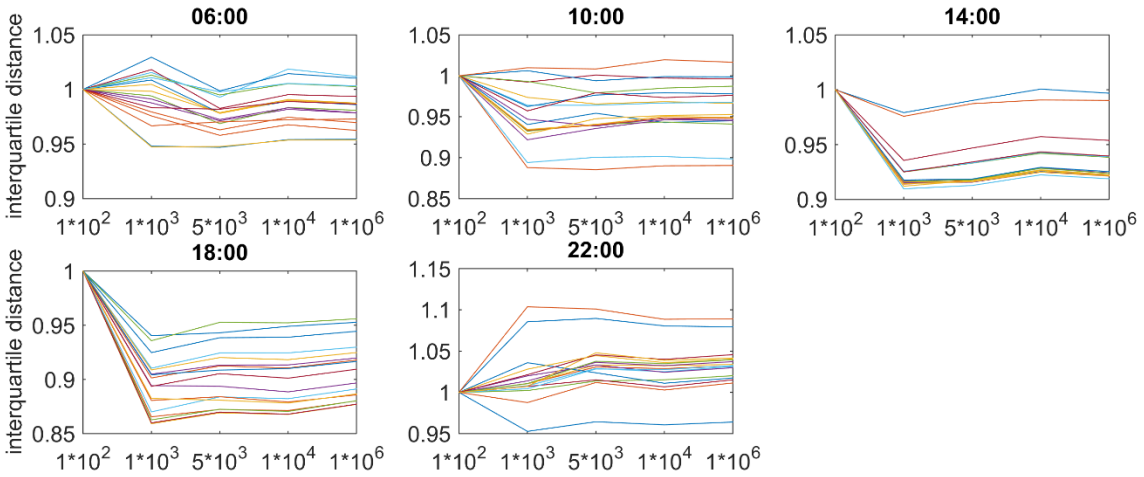

Figure 4 Interquartile distances of 10^2, 10^3, 10^4, 10^5 and 10^6 calculations of Jacobian matrices for each time point. The x-axis represents the number of repetitions of the inverse calculation. All distances were normalised to the interquartile distance of 100 replicates.

The diagonal Jacobian entries of alpha-ketoglutarate, $\delta f(kga)/\delta kga$, containing information about the influence of concentration changes on its own metabolic function, revealed a dramatic fluctuation at 18:00 (**Figure 5**). In general, at the time point 18:00, which corresponded to 12 hours of light in the diurnal period, almost all diagonal entries of Jacobian matrices reached a peak value (**Figure 5**).

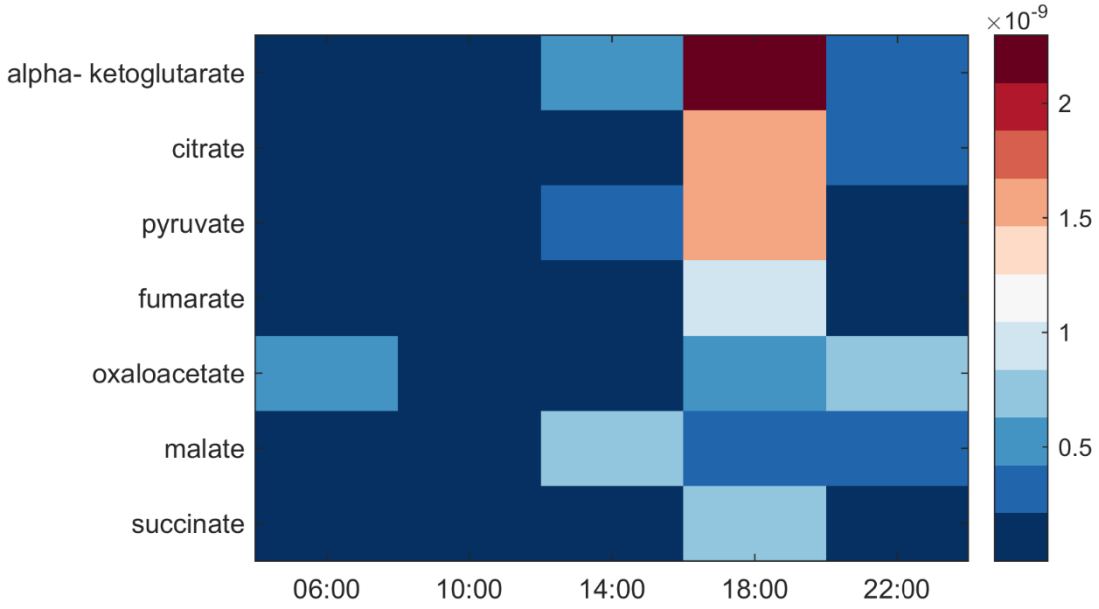

Figure 5 Diurnal dynamics of diagonal Jacobian Entries of the TCA cycle model, ranked after the highest entry. Colours represent absolute values of Jacobian Entries.

Ranking metabolites according to the absolute values of diagonal Jacobian entries, the first part of the cycle, i.e. pyruvate, citrate and alpha-ketoglutarate, was found to have consistently higher values at 18:00 than metabolites of the second part, i.e. succinate, fumarate, malate and oxaloacetate (**Table 3**).

Table 3 Diagonal Jacobian entries of metabolites in the TCA cycle model, ordered concerning the maximum value in the course of the light period.

	06:00	**10:00**	**14:00**	**18:00**	**22:00**
alpha- ketoglutarate	2.16E-12	2.07E-10	5.97E-10	2.30E-09	3.55E-10
citrate	3.58E-12	1.38E-10	3.09E-11	1.63E-09	2.88E-10
pyruvate	3.90E-11	3.12E-11	2.23E-10	1.61E-09	2.57E-11
fumarate	1.31E-11	2.44E-12	2.09E-10	9.99E-10	4.92E-11
oxaloacetate	4.64E-10	1.49E-11	7.15E-11	5.32E-10	8.37E-10
malate	2.79E-11	2.12E-11	7.74E-10	2.35E-10	2.87E-10
succinate	2.14E-11	3.36E-11	3.45E-11	6.99E-10	7.75E-12

The time dependent concentration of alpha- ketoglutarate showed a significant drop between 14:00 and 18:00 with a subsequent increase until 22:00, while in the first part of the day (06:00-14:00) a slight increase was observed (**Figure 6 - A**). The detailed visualisation of the diagonal Jacobian entries of alpha- ketoglutarate over the course of the day (**Figure 6 - B**) revealed smaller changes in the first three time points and a substantial peak at 18:00.

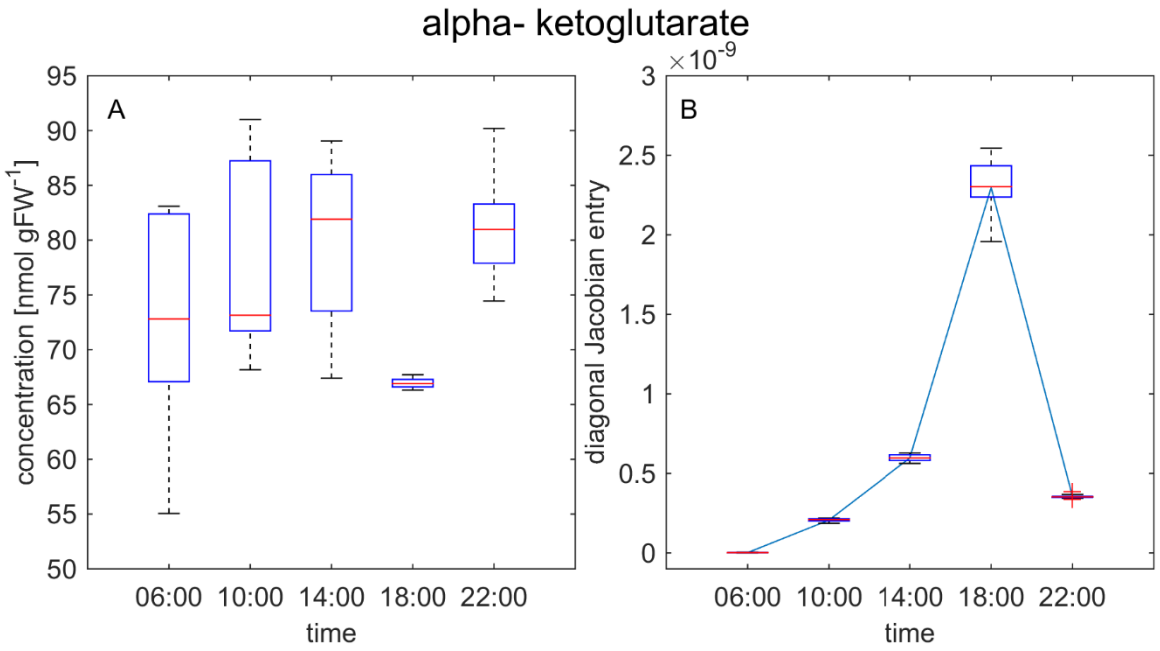

Figure 6 Diurnal dynamics of alpha- ketoglutarate concentrations (**A**) and the diagonal Jacobian entries (**B**). The blue line indicates the mean of the iterative calculations.

Due to large variances, the diurnal concentration dynamics of citrate did not feature statistically significant changes, but an increase at 10:00 with a subsequent decrease until 18:00 was observable (**Figure 7 – A**). The diagonal Jacobian entries, similar to alpha-ketoglutarate, showed a large peak at 18:00 and a smaller one at 10:00 (**Figure 7 – B**).

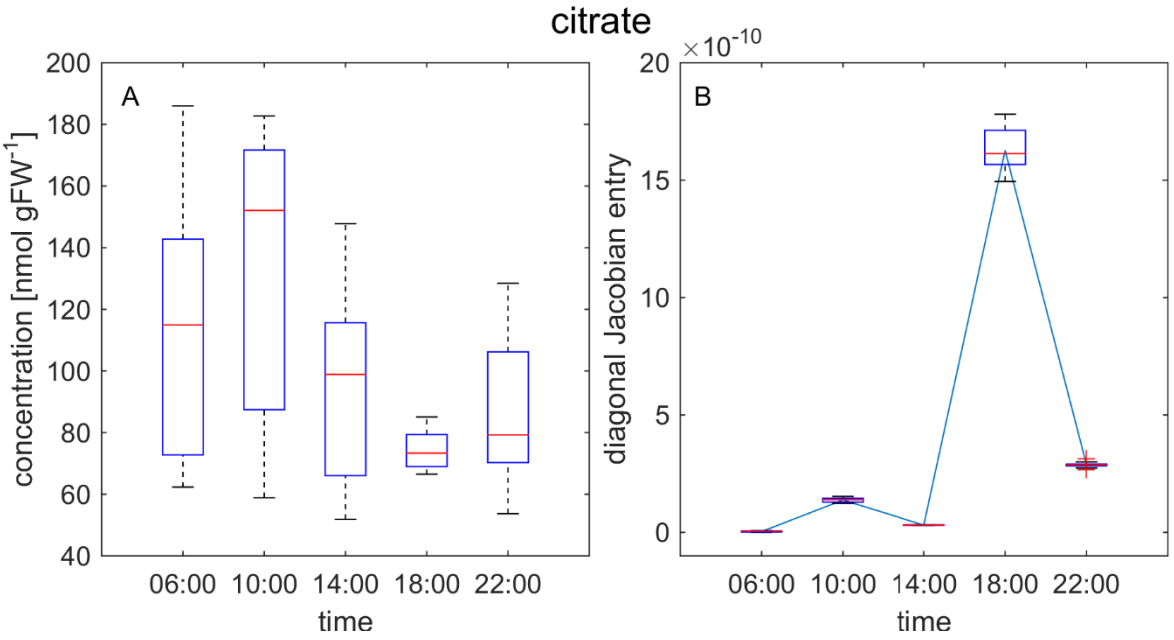

Figure 7 Diurnal dynamics of citrate concentrations (**A**) and the diagonal Jacobian entries (**B**). The blue line indicates the mean of the iterative calculations.

The concentration of pyruvate increased from 06:00 until 14:00, dropped at 18:00 and finally reached levels similar to the first half of the day at 22:00 (**Figure 8 – A**). The diagonal entries showed a similar pattern as alpha- ketoglutarate and citrate, featuring a distinct peak at 18:00 (**Figure 8 – B**).

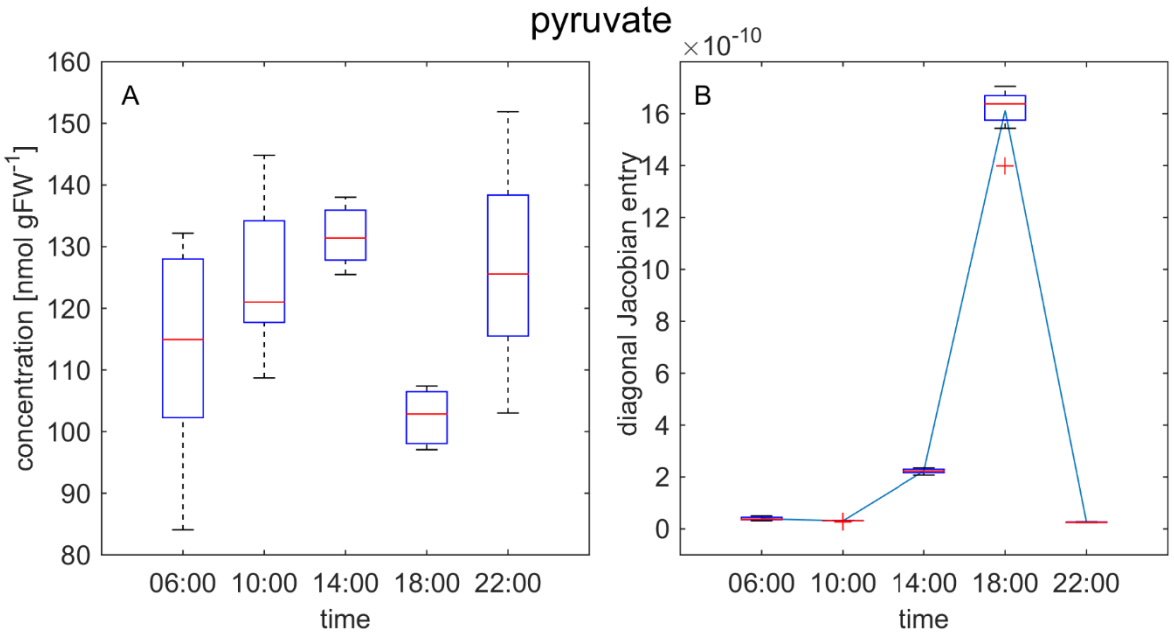

Figure 8 Diurnal dynamics of pyruvate concentrations (**A**) and the diagonal Jacobian entries (**B**). The blue line indicates the mean of the iterative calculations.

6.4. Simulation of the metabolic C/N interface

The minimum number of inverse calculations for a stable interquartile distance was determined as described for the TCA cycle model (see chapter 6.3). Most of the Jacobian entries showed stable interquartile distances after 1000 iterations (**Figure 9**). Yet, in order to overcome remaining fluctuations in some of the Jacobian entries, calculations were performed 10^4 times.

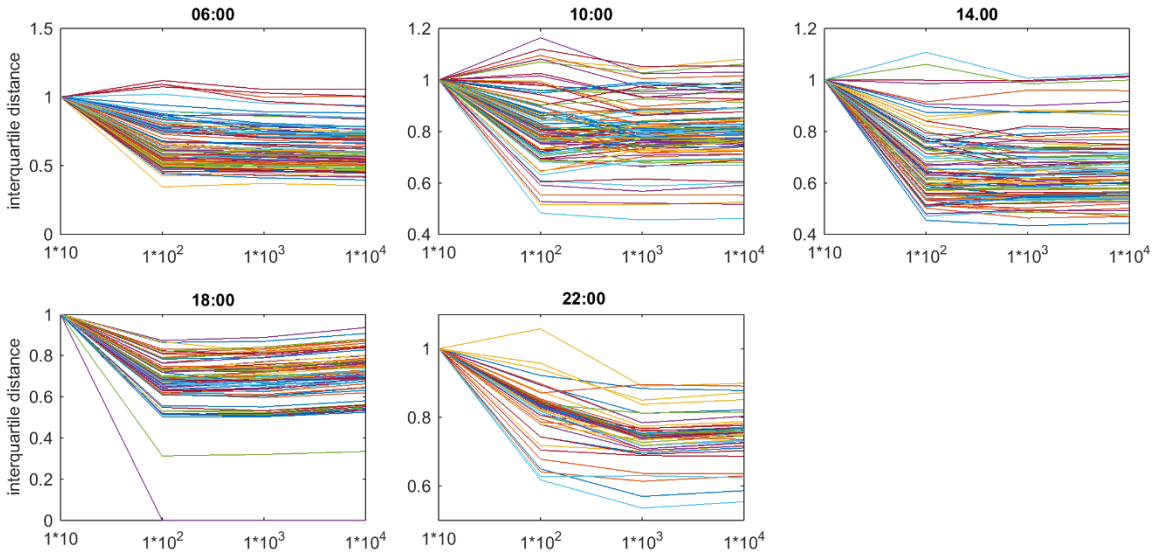

Figure 9 Interquartile distances of iterative calculations of Jacobian matrices. The x-axis represents 10, 10^2, 10^3 and 10^4 repetitions of the inverse calculation.

The analysis of all diagonal Jacobian entries over the diurnal time course indicated similar patterns of entries related to alpha- ketoglutarate, glutamate and glucose (**Figure 10**; Appendix **Table S2**). These three metabolites were clearly separated from the others, by showing notably higher diagonal Jacobian values. For a full representation of all Jacobian matrix entries for the interactions contained in the network see Appendix **Table S3**.

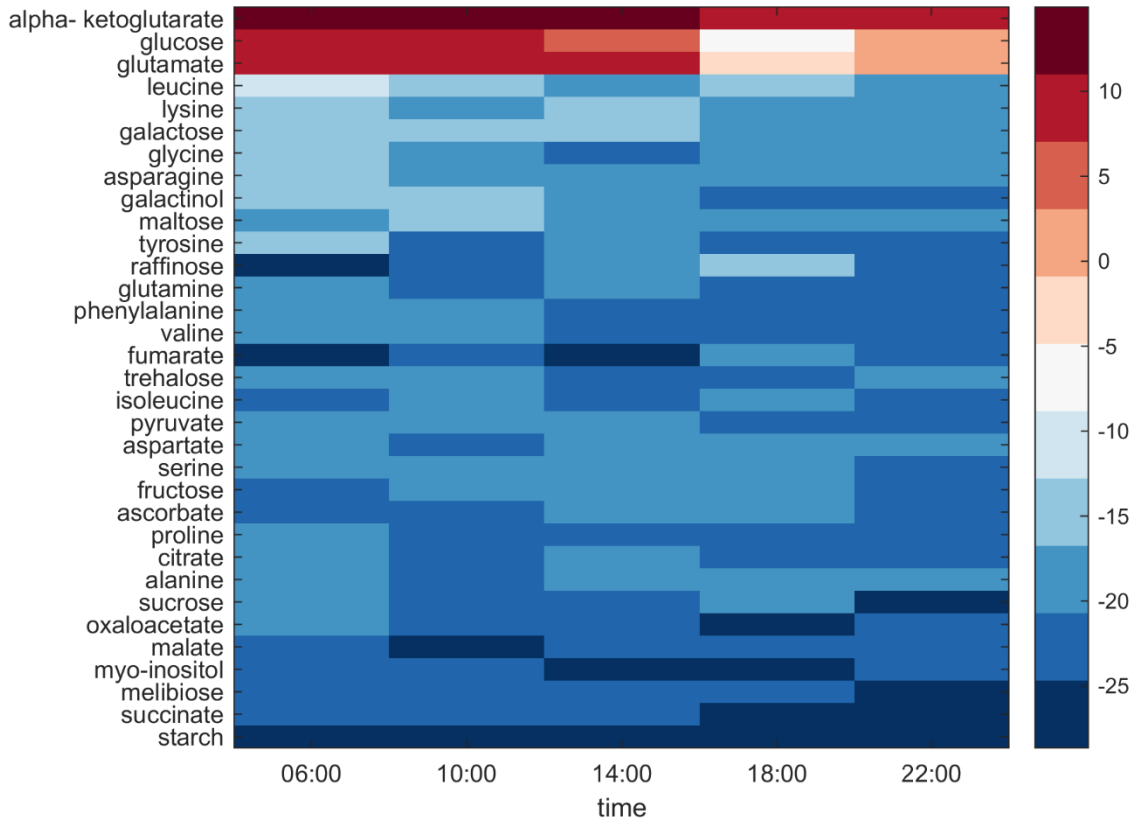

Figure 10 Diurnal dynamics of diagonal Jacobian entries, ranked after the highest entry. Colours represent absolute values on a log scale.

To unravel the influences of connected metabolite pools on the identified key regulators glutamate, alpha- ketoglutarate and glucose, all corresponding dependencies were investigated .

In detail, the diagonal entries of alpha- ketoglutarate increased during the first part of the day until 14:00 followed by a sharp decrease approaching values near to zero in the evening (**Figure 11 - A**), which was similar to the dynamic behaviour of the Jacobian entries of $\delta\, f(\alpha - kga)/\delta\, oxa$ (**Figure 11 - C**). The other non-diagonal entries featured a distinct peak at 14:00 (**Figure 11 – B, D, E**).

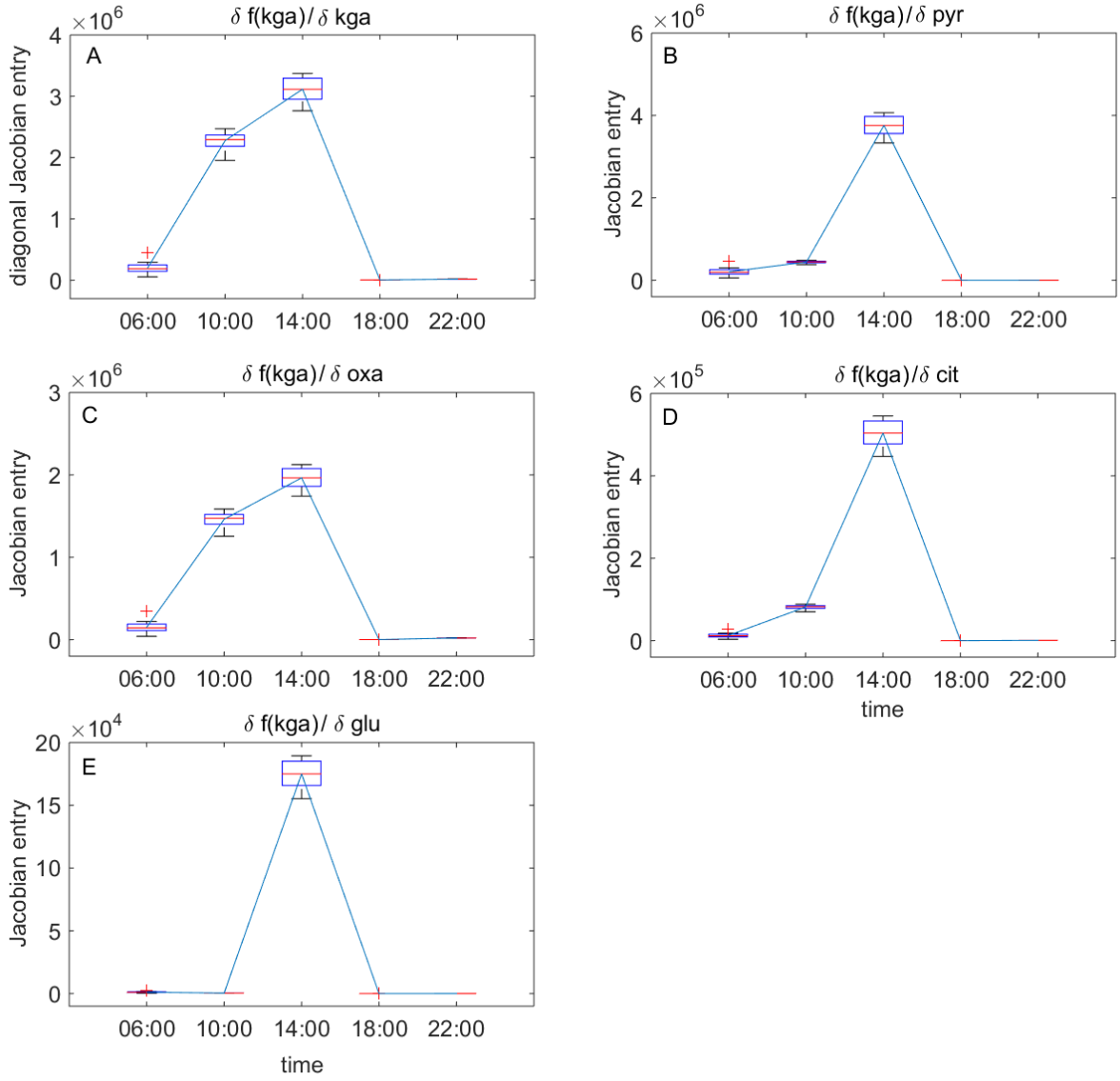

Figure 11 Diurnal dynamics of Jacobian entries describing the dependency of the alpha- ketoglutarate function on alpha- ketoglutarate (**A**), pyruvate (**B**), oxaloacetate (**C**), citrate (**D**) and glutamate (**E**)**.** Blue lines indicate the median of the calculations.

Diurnal dynamics of glutamate concentration were characterised by a slight increase during the first four hours of the day, which was followed by a sharp decrease at 14:00 (**Figure 12**). Additionally, the variance of the pool was found to be smallest at time point 14:00 which represents the middle of the light period.

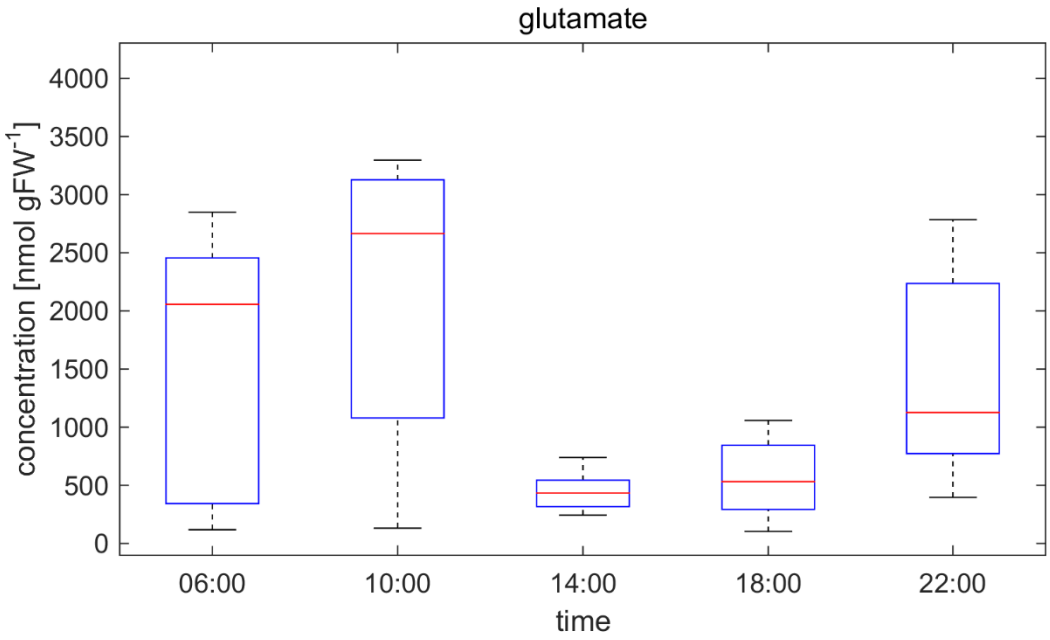

Figure 12 Diurnal dynamics of glutamate concentrations

A clear increase of the diagonal Jacobian entries of glutamate was detected during the first four hours of the light period, while they decreased almost to zero during the evening (**Figure 13 –A**). The non-diagonal entries featured high values in the beginning of the day, which decreased until evening (**Figure 13 – B-F**). Additionally, the entries of $\delta\, f(glu)/\delta\, kga$ and $\delta\, f(glu)/\delta\, oxa$, showed an increase in the middle of the day, at 14:00.

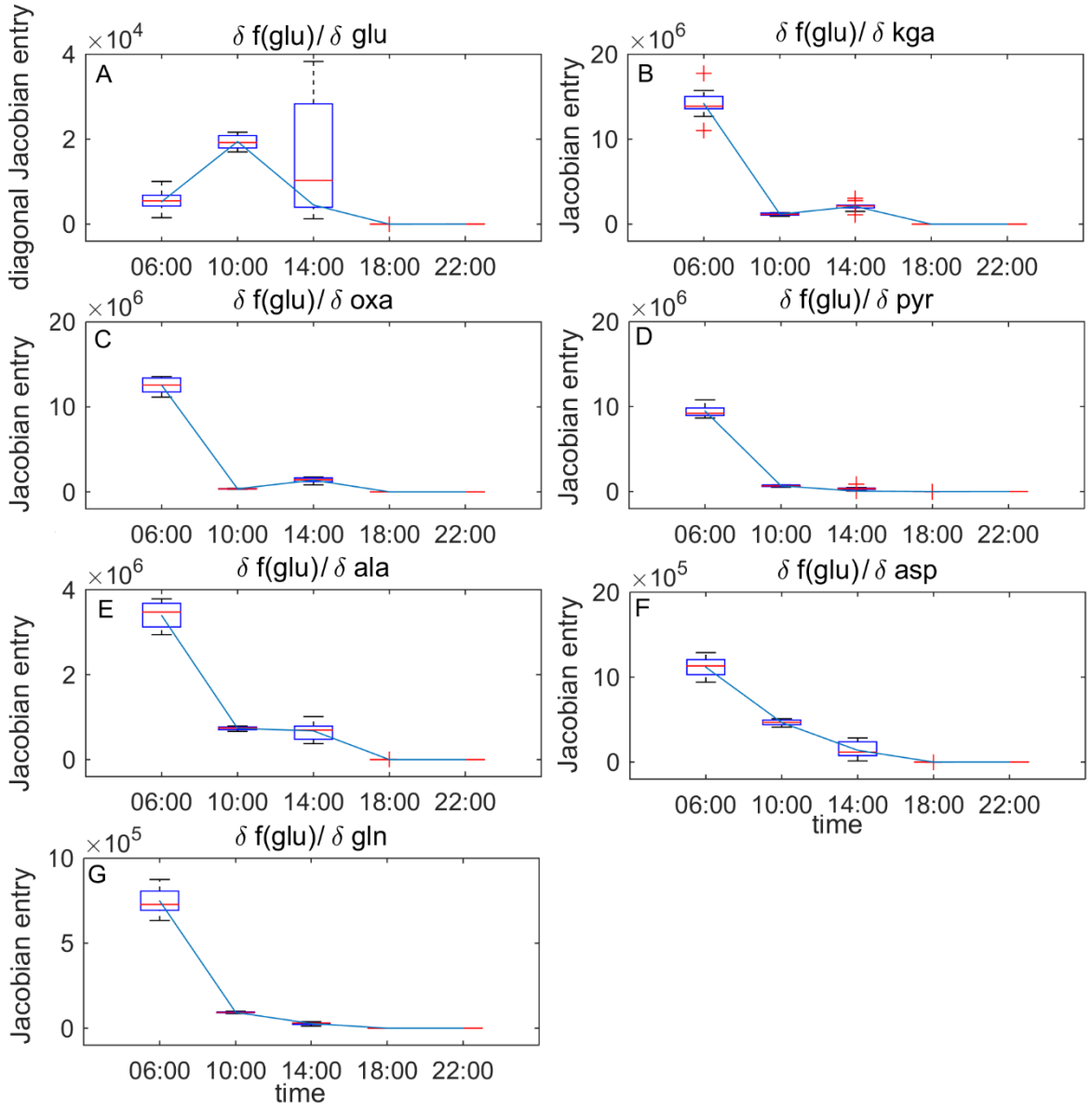

Figure 13 Diurnal dynamics of Jacobian entries describing the dependency of the glutamate function on the concentration of glutamate (**A**), alpha- ketoglutarate(**B**), oxaloacetate (**C**), pyruvate (**D**), alanine (**E**), aspartate (**F**) and glutamine (**G**). Lines indicate the median of the calculations.

The interaction with oxaloacetate was shown to be important for both alpha- ketoglutarate and glutamate (**Figure 11- C and Figure 13- C**). The only reaction where these metabolites interact in the examined context is the biosynthesis of aspartate (see **Figure 2**). The Jacobian entries describing the aspartate function with respect to changes in concentrations of glutamate and oxaloacetate showed a peak value in the middle of the light period at 14:00 (**Figure 14**).

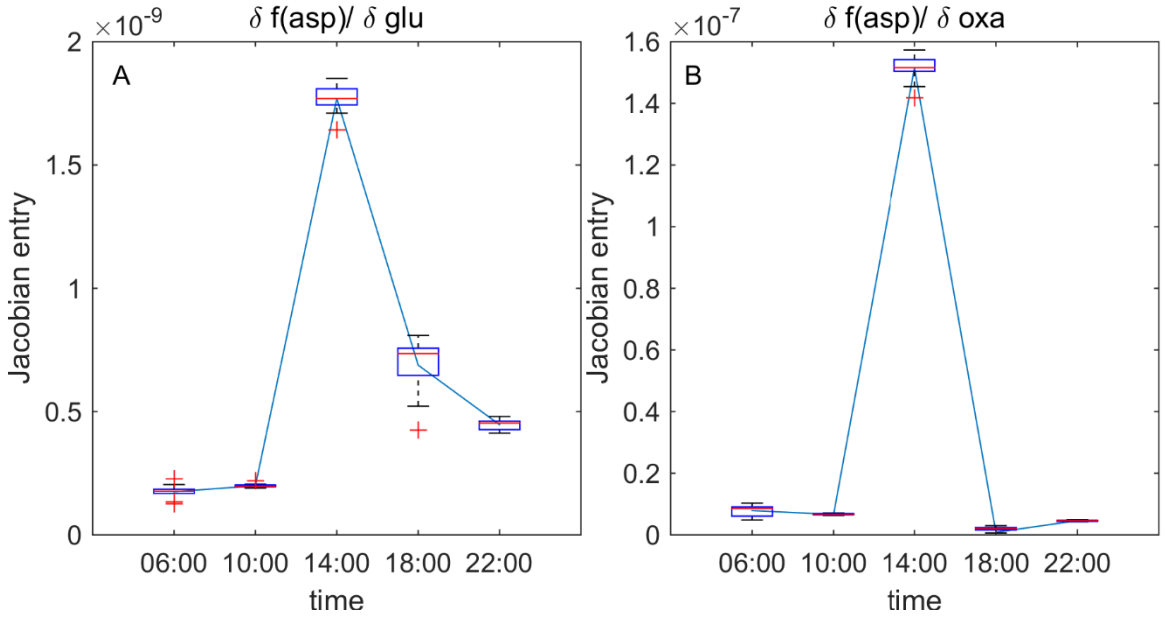

Figure 14 Diurnal dynamics of absolute Jacobian entries for the metabolic function of aspartate depending on the concentration of glutamate (**A**) and oxaloacetate (**B**). Lines indicate the mean of the iterative calculations.

The concentration of aspartate was found to be rather constant during the diurnal cycle although a decrease of variance was observed in the pool between 14:00 and 18:00 (**Figure 15**). The median concentration of oxaloacetate increased by until 14:00 followed by a considerable decline. Finally, between 18:00 and 22:00 the concentration rose again to a similar level as observed at 14:00 (**Figure 16 -A**). The diagonal Jacobian entries were high in the morning, dropped at 10:00 and showed a second peak at 14:00. In the evening they were close to zero (**Figure 16 -B**).

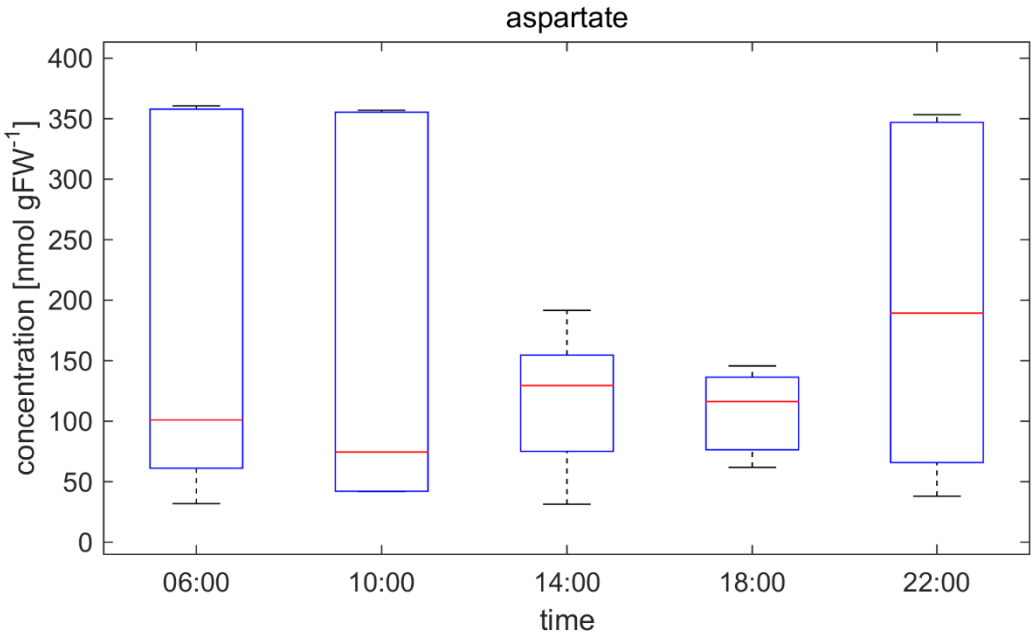

Figure 15 Diurnal dynamics of aspartate concentration.

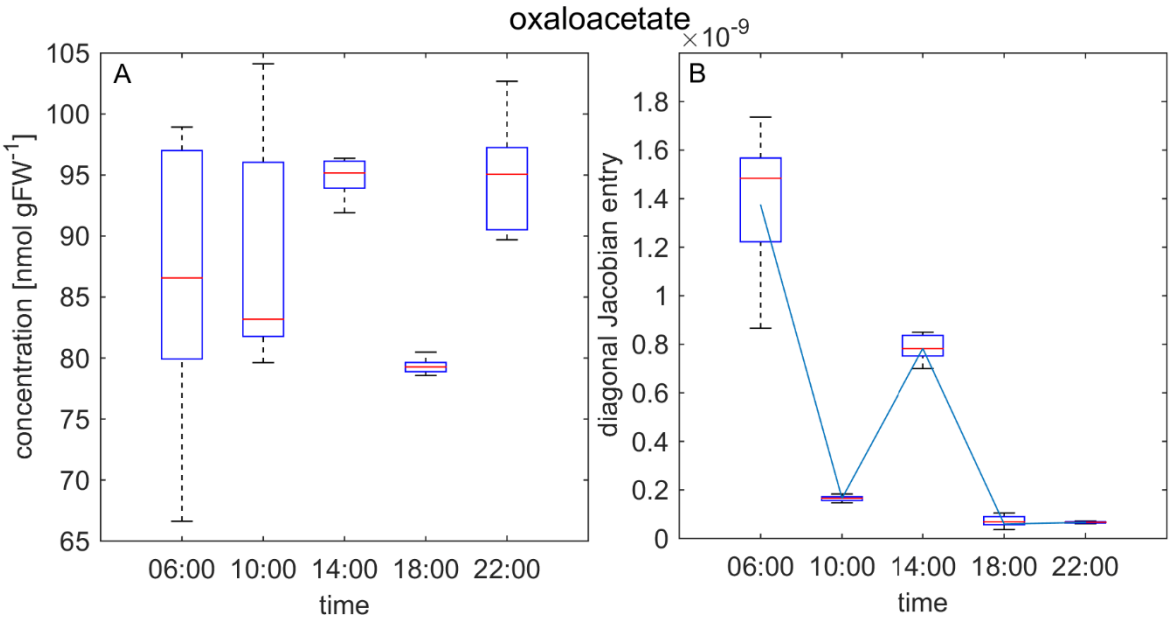

Figure 16 Diurnal dynamics of oxaloacetate concentration (**A**) and the diagonal Jacobian entries (**B**). The blue line indicates the mean of the iterative calculations

The next essential interactions of glutamate are with pyruvate and alanine (**Figure 13 – D, E**). The concentration of alanine did not show any significant changes during the light period, but seemed to increase slightly at 10:00 and 22:00 (**Figure 17**).

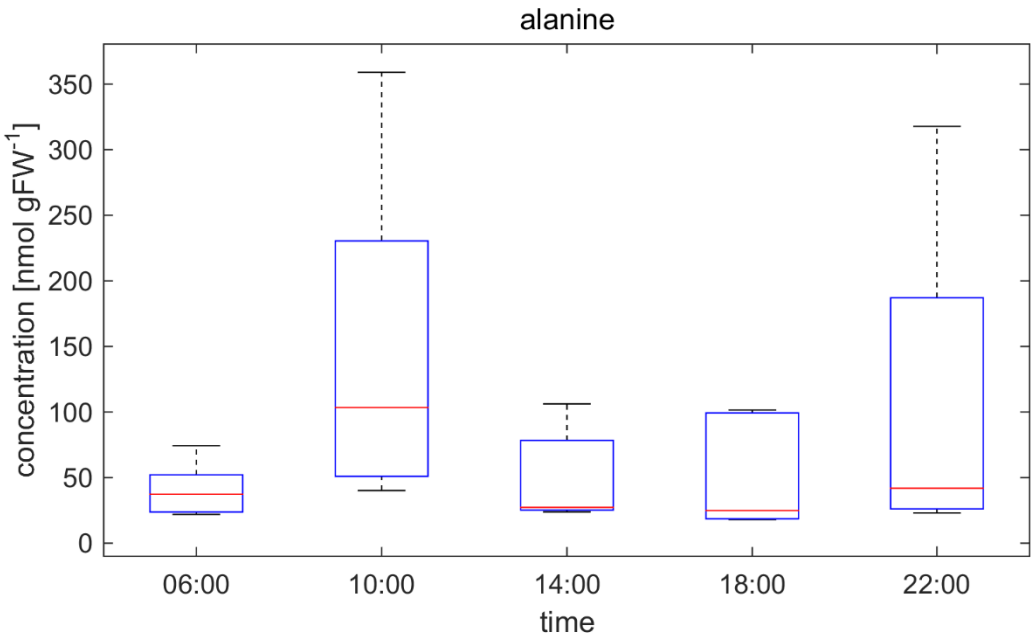

Figure 17 Diurnal dynamics of alanine concentration.

The dependency of the alanine metabolic function on the pyruvate pool shows a distinct increase in the middle of the day with a following decrease until the end of the light phase (**Figure 18**).

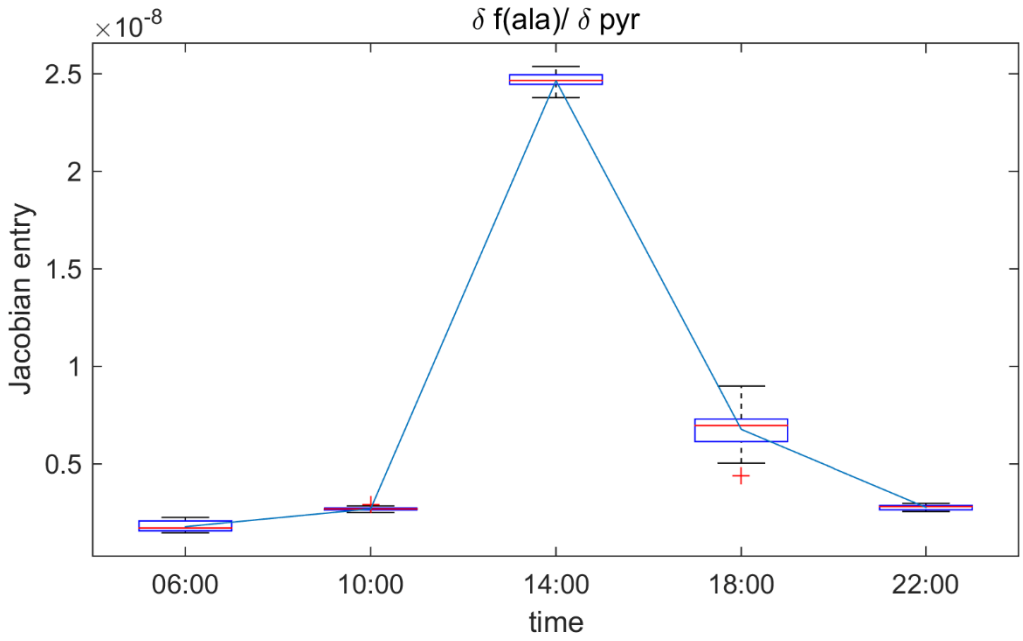

Figure 18 Diurnal dynamics of Jacobian entries describing the dependency of the alanine function on the pyruvate concentration. The line indicates the mean of the iterative calculations.

The concentration of glucose showed a dramatic peak at 10:00, with a subsequent decrease, so the levels at 14:00 are similar to 06:00, finally from 14:00 to 22:00 the concentration increased slightly (**Figure 19**).

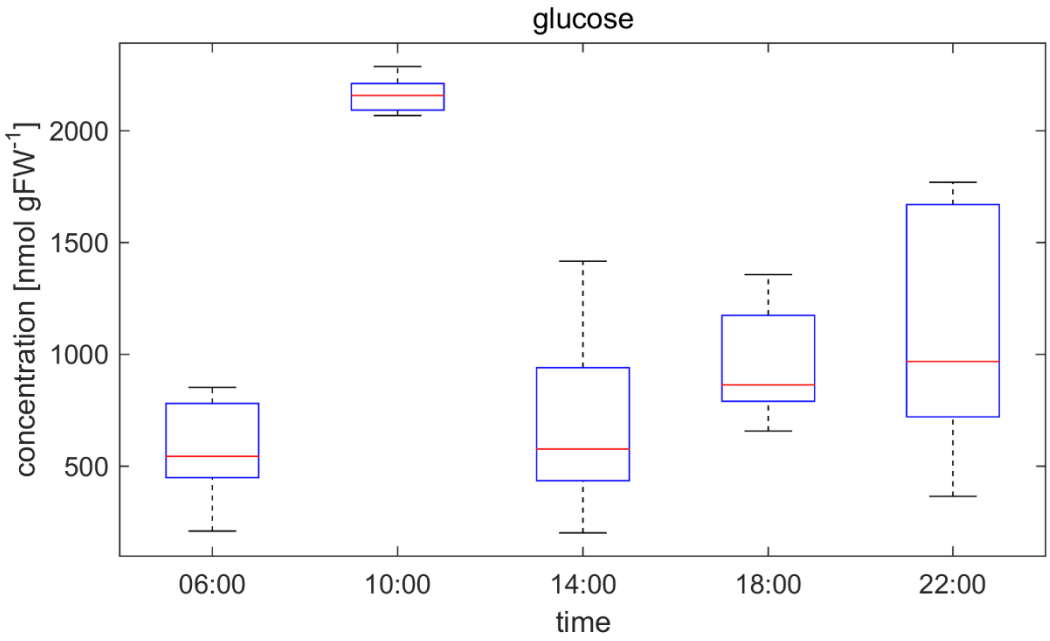

Figure 19 Diurnal dynamics of glucose concentrations.

The diagonal Jacobian entries of glucose featured a high value in the morning, followed by a rapid decrease to almost zero until 14:00. In the second half of the day the values remained low (**Figure 20 - A**). The non-diagonal entries featured similar diurnal dynamics (**Figure 20 B-E**), with the exception of $\delta\ f(glc)/\delta\ mlt$, which showed rather stable values until 10:00 with a subsequent, distinct decline to 14:00.

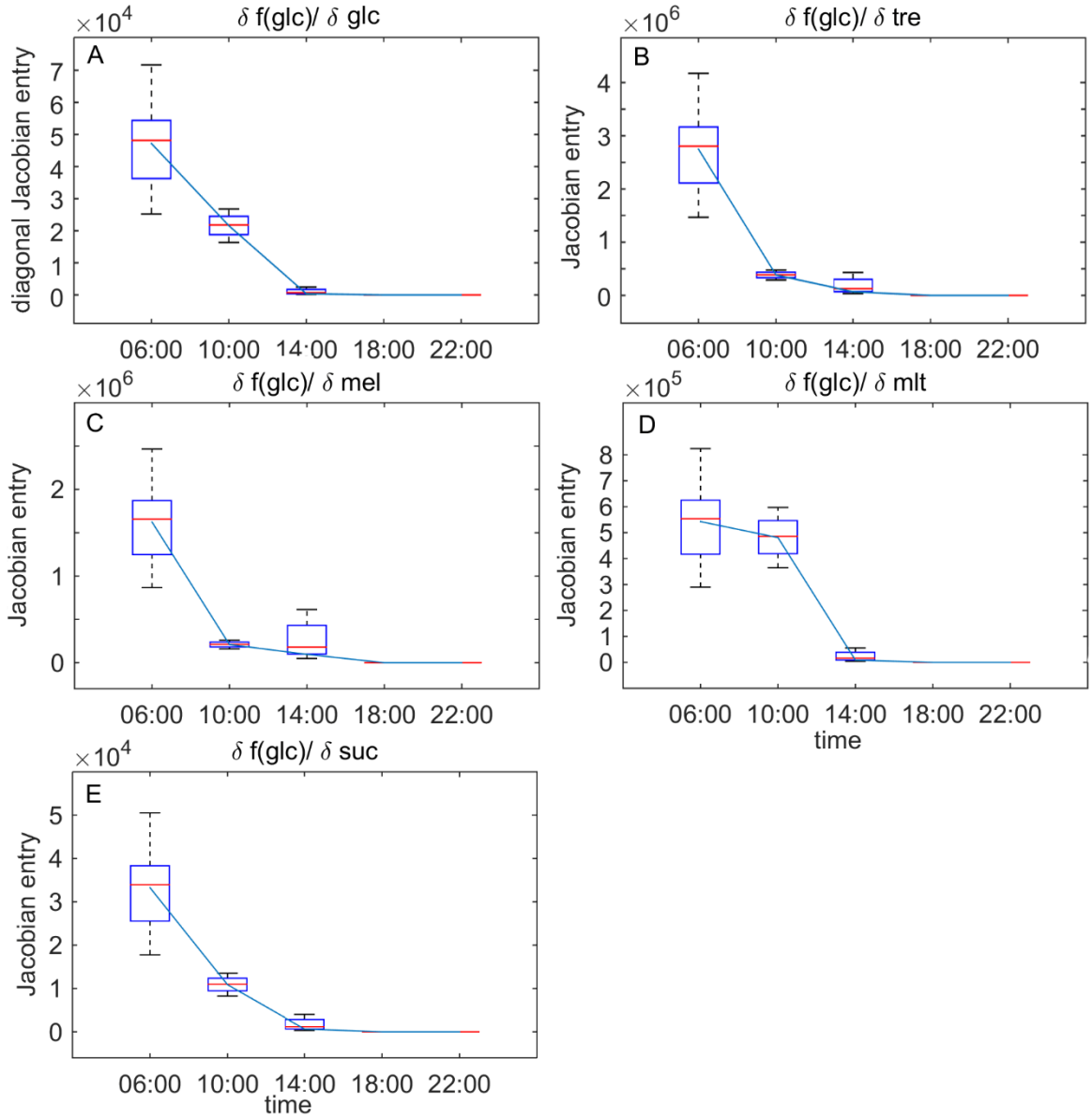

Figure 20 Diurnal dynamics of Jacobian entries describing the dependency of the glucose function on the concentration of glucose (**A**), trehalose (**B**), melibiose (**C**), maltose (**D**), and sucrose (**E**). Blue lines indicate the median of the calculations.

In addition to the identified key element glucose, the starch metabolism was examined. Transitory starch levels increased until a plateau at 18:00 was reached (**Figure 21 - A**), while the diagonal Jacobian entries of starch metabolism were found to be higher in the morning, and close to zero in the afternoon, with a small increase at 14:00 (**Figure 21 - B**). In general, the diagonal Jacobian entries of starch metabolism had a very low absolute value (10^{-11}). The Jacobian entries of $\delta\ f(mlt)/\delta\ sta$ showed a decrease in the beginning of the day and then stayed low until evening (**Figure 22**).

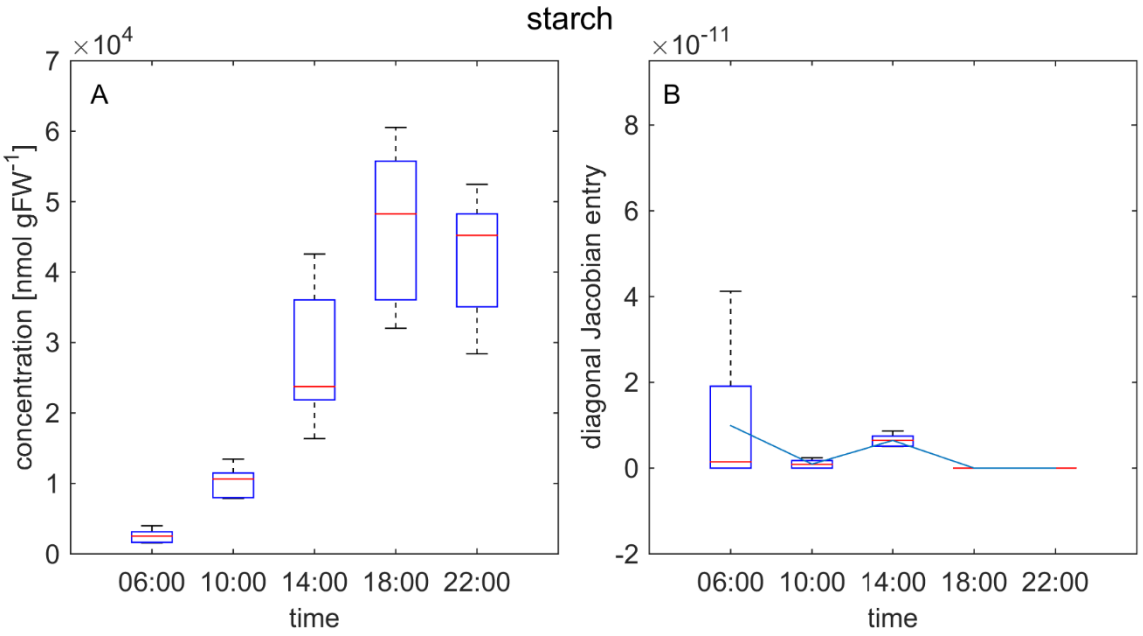

Figure 21 Diurnal dynamics of transitory starch concentrations (**A**) and the diagonal Jacobian entries (**B**). The blue line indicates the mean of the iterative calculations.

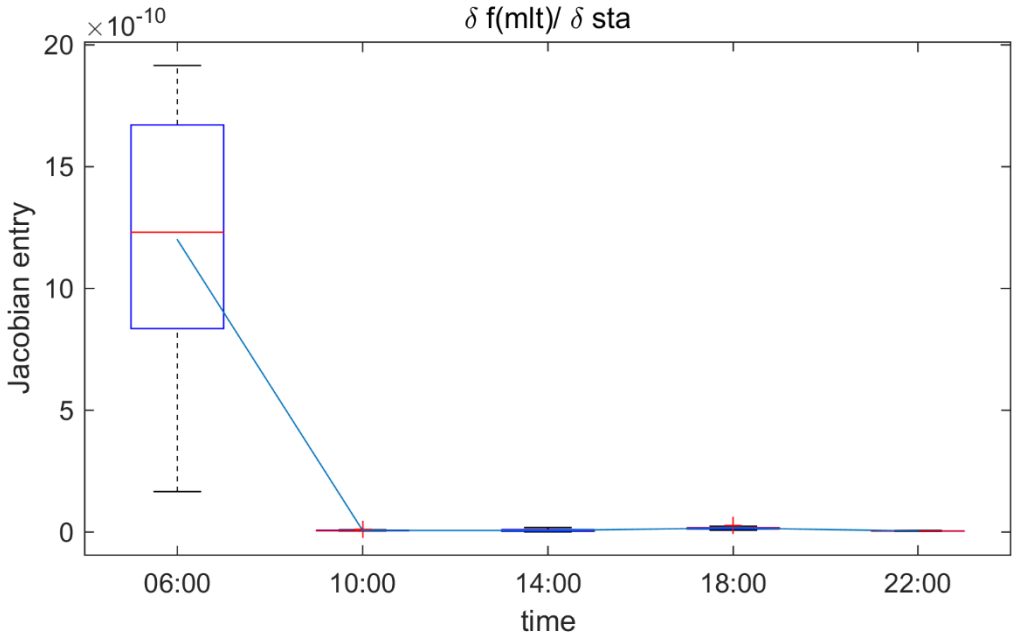

Figure 22 Diurnal dynamics of the Jacobian entries describing the dependency of the metabolic function of maltose on the transitory starch pool. The line indicates the mean of the iterative calculations.

7. Discussion

7.1. The development of a high confidence network is imperative for metabolic modelling

In the present work, a theoretical method was developed which allows for the extraction of meaningful biochemical networks from genome scale metabolic network reconstructions. A user friendly GUI was programmed to ease and support future modelling approaches (Appendix - **Figure S2** and **Figure S3**). As previously mentioned, it is imperative that every single reaction contained in a metabolic network, needs to be carefully examined and validated by available literature sources (see chapter 4.5). Particularly, enzymes catalysing rate limiting steps of metabolic interconversion should be included in the reduced model structure in order to preserve the biochemically and physiologically relevant network information. Even if large scale metabolic reconstructions are available, they are often algorithm generated and contain a comprehensive set of reactions predictable by the genome in an organism (see e.g. (Thiele & Palsson, 2010)). As the covariance based modelling approach presented in this work relies on the validity of the biochemical interaction matrix, only reactions which are well characterized and can be confidently predicted in the organism should be included.

7.2. Jacobian matrix entries represent tangents of biochemical reaction rates

A Jacobian matrix entry comprises information about the influence of changes in a metabolite concentration on a specific metabolic function, which allows to draw conclusions about the dynamic capabilities of an underlying biochemical system. More specifically, a large entry indicates that even a small change in a metabolite concentration can have a significant influence on the metabolic function. If Michaelis Menten kinetics are assumed for the reaction with the largest influence on the metabolic function, this dependency can be visualized as depicted in **Figure 23**. If tangents, which represent a linearization of a function in a certain point, are drawn at certain substrate concentrations, e.g. 20 [arbitrary units – a.u.] (**Figure 23-A**) and 10 [a. u.] (**Figure 23–B**) on the reaction rate function, it becomes evident that a small change in the substrate concentration has a stronger effect when the enzyme is not saturated. Hence, a decrease in substrate concentration is one possible explanation for an increase in a Jacobian matrix value. Another explanation for a Jacobian value alteration is the change of

enzyme abundance. Thus, a small change in substrate concentration has a stronger effect on the reaction rate if more enzyme is available, because the enzyme is farther away from being in a saturated state (**Figure 23-C**, orange line).

If none of the previously mentioned scenarios seem to be able to explain a change in the Jacobian matrix values, it could be that the dependencies are shifted due to allosteric interactions.

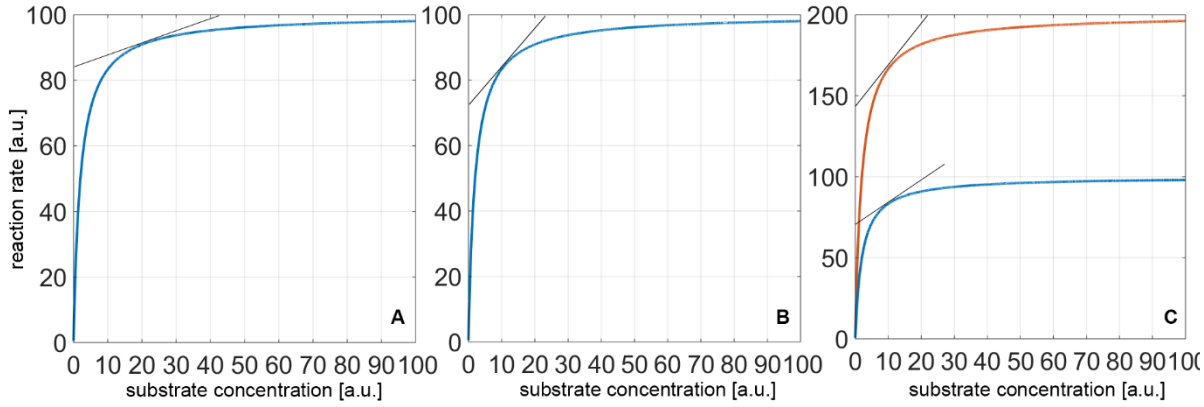

Figure 23 Ideal Michaelis-Menten kinetics for an exemplary enzyme. Tangents show the linearization of the reaction rate at a certain substrate concentration. Tangent at substrate concentration 20 [arbitrary units – a.u.] (**A**), Tangent at substrate concentration 10 [a.u.] (**B**), both tangents at substrate concentration 10 (**C**), the orange line indicates a doubled maximal reaction rate (v_{max}), representing, e.g. an increased enzyme concentration.

When discussing the Jacobian entries acquired through covariance-based calculation methods, it should be kept in mind that the Jacobian matrix describes a metabolic steady state. Therefore it is possible to approximate the Jacobian matrices through inverse calculation at the time points of measurement, but an extrapolation over the whole time course would not be valid. Thus, the transitions between the calculated time points were assumed to be linear for graphical representation (e.g. **Figure 6 B**), which is reasonable in the way, that it does not change the interpretation of the results.

7.3. Alpha- ketoglutarate acts as a key regulator in diurnal energy metabolism

The TCA cycle is of particular biochemical interest, because it is a central hub of primary metabolism. Therefore, identified patterns of regulation may provide insight into fundamental

mechanisms of plant growth and survival. Secondly, it poses a special challenge for modelling approaches because the explanation of regulatory effects may always incorporate some redundancy due to propagating regulation effects in cyclic structures.

Through the analysis of diagonal Jacobian entries of all metabolites in the TCA cycle, alpha-ketoglutarate was identified as the most important biochemical regulator in a diurnal context, followed by citrate (**Table 3** and **Figure 5**). In early studies about metabolic fluxes through the TCA cycle it was also found that alpha- ketoglutarate dehydrogenase and citrate synthase act as key regulators (Safer & Williamson, 1973).

Almost all diurnal time-courses of metabolites contained in the TCA model showed a peak in their diagonal Jacobian entries at 18:00, which gave the impression that this time point was an important point of regulation in the TCA cycle or possibly even other catabolic processes like mitochondrial respiration. Due to the major part of respiration taking place in the dark (Schopfer & Brennicke, 2010), it was interesting to see such a change in dependencies already in the evening when light was still available. These changes could indicate steps of metabolic reprogramming for the upcoming dark phase which would enable an efficient and quick switch from light regulated to dark regulated processes. Such a change in energy metabolism was also suggested by the change in starch metabolism indicated by the constant starch levels from 18:00 to 22:00 (**Figure 21**).It has been shown that under long-day conditions, i.e. 16h light/8h dark, the estimated growth of the plants, and therefore their carbon allocation profile, shows a sinusoidal form with two peaks where the second peak appears already at predawn (Sulpice et al., 2014).

When the diurnal dynamics of the diagonal Jacobian entries for alpha- ketoglutarate and its change in total concentration were evaluated (**Figure 6**), the peak at 18:00 could be partially explained by the decrease in concentration and variance of the metabolite. Due to the assumption of Michaelis Menten kinetics for the alpha- ketoglutarate dehydrogenase reaction, which is most likely the regulating step for this metabolite pool (Tretter & Adam-Vizi, 2005), a decrease in concentration would increase the influence of variations in the metabolite pool on the metabolic function (see chapter 7.2). However, this would not explain the rise of the diagonal entries in earlier time points as the concentration was rather increasing, though not significantly. One hypothesis of how such a pattern may arise would be an increased abundance of the enzyme level during the day and, by this a change in metabolite concentrations would lead to a stronger effect on the metabolic function. The validity of this

hypothesis was supported by proteomics data, which showed that the alpha- ketoglutarate dehydrogenase protein had a higher abundancy in the evening than in the morning (**Figure S1**) (E. Nukarinen, unpublished data). Additionally, it has been shown that the expression of two alpha- ketoglutarate dehydrogenase genes (AT5G65750, AT3G55410) increases during the day and decreases during the night (Blaesing et al., 2005; Mockler et al., 2007; S. Smith et al., 2004).

Citrate and pyruvate, which were identified as the following important regulators (**Table 3**) showed very similar patterns in their diagonal Jacobian entries as alpha- ketoglutarate (**Figure 5**). The peak in the diagonal Jacobian entries of citrate at 18:00 might be explained by the observed decrease in concentration and variance of citrate at this time point (**Figure 7**). This is also valid for the diagonal Jacobian entries of pyruvate, as the concentration features a similar decrease at 18:00 (**Figure 8**). The expression of pyruvate kinase (AT2G36580) and aconitase (AT2G05710) showed similar patterns, indicating an increase during the day and a decrease during the night (Mockler et al., 2007; S. Smith et al., 2004).

7.4. Glutamate-dependent aminotransferase reactions show a distinct diurnal pattern

Model A (**Figure 2**) contained all metabolites which were absolutely quantified by GC-MS analysis covering the central primary metabolism in *Arabidopsis thaliana*. Results indicated that the three most important key elements in the diurnal regulation of primary metabolism were alpha- ketoglutarate, glucose and glutamate (**Figure 10** and **Table S2**). The identification of alpha- ketoglutarate as a key biochemical regulator agreed with the results of the TCA cycle model (see chapter 6.3). Alpha-ketoglutarate and glutamate pools were known to be tightly interconnected via several biochemical pathways (Schopfer & Brennicke, 2010). Moreover, they directly affect the carbon-nitrogen homeostasis of a plant. Their identification as key elements was therefore meaningful, indicating the biochemical validity and interpretability of the results gained by the modelling approach. In plants, the regulation of sugar levels is strictly controlled (see e.g. (Rolland, Baena-Gonzalez, & Sheen, 2006)), which could be a reason for the observed pattern of glucose regulation. Additionally, it has been shown that glucose serves as a key regulator in various processes and is a central signalling molecule in plants (Blaesing et al., 2005; Moore et al., 2003; Rolland, Moore, & Sheen, 2002).

Comparing Jacobian entries of the two different models it was necessary to differentiate two different biochemical backgrounds. In model B, the mitochondrial tricarboxylic acid cycle, and hence, only mitochondrial influences were considered while model A contained additional reactions from amino acid biosynthesis pathways and central carbon metabolism.

Model A is more applicable to the presented dataset, as the metabolite concentrations were determined without prior separation of subcellular compartments and it has been shown that TCA cycle intermediates are not only part of the mitochondrial metabolism but also take part in reactions of other compartments, e.g.: fumarate can serve as an alternative carbon sink under high nitrogen conditions (Pracharoenwattana et al., 2010). Though, Model B could still give important information about the regulation of the mitochondrial TCA cycle.

The shift of the peak in alpha- ketoglutarate diagonal Jacobian entries from 18:00 in model B (**Figure 6** and **Figure 11**) to an earlier point in the day in model A could be an indication of the increased influence of nitrogen metabolism on the regulation of this metabolite pool. This directly supports the hypothesis of a high influence of nitrogen metabolism during the day, which was reported by several studies. For example, in tobacco plants the total amount of amino acids was found to be significantly lower if the plant had been exposed to short day conditions (Matt, Schurr, Klein, Krapp, & Stitt, 1998). In *Arabidopsis* the concentration of amino acids was reported to increase throughout the day and to decrease slightly in late evening (Sulpice et al., 2014). However, in a plant, the total concentration of amino acids alone might not be sufficient to estimate the dynamics of amino acid metabolism, as they are not just end products and used for storage, but continuously processed in the construction of proteins and therefore undergo a constant turnover (Bauer, Urquhart, & Joy, 1977). This raised the question which reactions might be limiting in these pathways and if their patterns of activity show diurnal changes. In many of the amino acid synthesis pathways glutamate acts as nitrogen donor and therefore, limits the rate of many different amino acids.

Plants take up most of the required nitrogen in the form of nitrate, which first needs to be reduced to ammonium, to be incorporated in the glutamine synthetase-glutamate-synthase pathway (GS-GOGAT). The activity of nitrate reductase, which catalyses the reduction of nitrate to nitrite and represents the first step in the reduction of plant usable nitrogen, was reported to increase as soon as light is cast on the plant and then decrease until evening in tobacco (Scheible, Krapp, & Stitt, 2000). This pattern of a high value in the morning and a decrease during the day could also be observed in the Jacobian entries, $\delta\, f(glu)/\delta\, gln$ and

$\delta\, f(glu)/\, \delta\, kga$ (**Figure 13**), describing the metabolic interconnection arising from the glutamine synthase and glutamate synthase reactions, which are following steps in the process of nitrogen uptake.

Another central reaction in plant amino acid metabolism is the transfer of an amino group from glutamate to oxaloacetate to form aspartate. This step is catalysed by the enzyme aspartate aminotransferase (EC 2.6.1.1). In the present study, the connection of oxaloacetate with glutamate and alpha- ketoglutarate could be identified as an important reaction in the diurnal dynamics of primary metabolism (**Figure 11 – C, Figure 13 - C**). Aspartate serves as amino group donor in several other pathways, like the biosynthesis of asparagine, methionine, threonine or lysine (Berg, Stryer, & Tymoczko, 2015) and is an important transport form of nitrogen from source to sink tissues. The mean level of aspartate was found to be constant over the diurnal period, but the variance was found to be lower at the time points 14:00 and 18:00, which already indicated a very tight regulation of the metabolite pool at these time points (**Figure 15**). Considering the dependencies of the aspartate metabolic function on the metabolite concentrations of glutamate and oxaloacetate, a strong peak could be identified in the middle of the day (**Figure 14**). This indicates that the rate of this transamination reaction was increasing until midday and then decreased until evening, which could also be representative and deducible for other amino acid biosynthesis reactions, which require aspartate as a substrate, e.g.: lysine biosynthesis.

The diurnal enzymatic activity of aspartate aminotransferase in *Arabidopsis* was monitored by Gibon and co-workers who found an increase from morning to midday and a decrease until evening (Gibon, Blaesing, Hannemann, et al., 2004). This described enzyme activity fit the observed pattern in the Jacobian entries $\delta\, f(asp)/\, \delta\, glu$ and $\delta\, f(asp)/\, \delta\, oxa$ (**Figure 14**), and it would explain that a change in the concentration of the two substrates had a large effect on the aspartate function during midday. Furthermore, this reaction seemed to be more limited by the amount of available oxaloacetate as the corresponding Jacobian entries $\delta\, f(asp)/\delta\, oxa$ were significantly higher than the entries $\delta\, f(asp)/\delta\, glu$ ($p<0.045$). Additionally, the diagonal Jacobian entries for oxaloacetate showed another peak at 14:00, which was most probably linked to the aspartate aminotransferase reaction (**Figure 16 - B**).In contrast, glutamate diagonal entries did not show such a peak (**Figure 13 - A**). The lack of this glutamate peak could be interpreted in two ways: (i) reactions with the most influence on the glutamate pool at this time point were either running at maximum capacity, or (ii) were limited

by another factor. The hypothesis that the glutamate pool is not the limiting factor for amino acid biosynthesis was also discussed in a previous study where Stitt and colleagues supplied plants with glutamate and could not observe an increase in other amino acids (Stitt et al., 2002).

A second glutamate consuming reaction in amino acid metabolism is the branch of alanine biosynthesis where an amino-group is transferred to pyruvate. The dependency of the alanine metabolic function on the pyruvate pool, which gave information about the reaction catalysed by an alanine aminotransferase (EC 2.6.1.2.), increased until midday and then declined until the end of the day. This pattern was similar to the regulation observed for the aspartate aminotransferase reaction. Additionally, the entries $\delta f(kga)/\delta pyr$, which correspond to the alanine biosynthesis showed the same pattern (**Figure 11 - B**). Based on this observation it is hypothesised that the activity of alanine aminotransferase behaves in a similar way as aspartate aminotransferase. This hypothesis also matches the results of Gibon and co-workers who found the activity of both enzymes to peak at midday (Gibon, Blaesing, Hannemann, et al., 2004). The derived hypothesis of a strong activation of amino acid biosynthesis was further supported by a significant peak in the entries $\delta f(kga)/\delta glu$, which show the dependency of the alpha- ketoglutarate function on the glutamate concentration (**Figure 11 - E**). This observed interconnection might also be due to the sudden decrease of the glutamate concentration at 14:00, which could be the effect of a high activity of transamination reactions using glutamate as amino group donor. This directly supports the hypothesis about the coordinated aspartate aminotransferase and alanine aminotransferase activity. As previously mentioned, the lack of corresponding peaks in the concentrations of aspartate and alanine (**Figure 15** and **Figure 17**) does not necessarily contradict the hypothesis of increased enzyme activities, but might rather be an indication of a high turnover of these amino acids.

The regulatory influence of glucose, indicated by the diagonal entries $\delta f(glc)/\delta glc$, seemed to be high in the morning and diminished as the day progressed, while the concentration of glucose increased (**Figure 19** and **Figure 20**). Additionally, the dependency of the glucose metabolic function on other metabolites decreased in a similar pattern during the day. While glucose is involved in numerous metabolic and regulatory processes in plant metabolism, it is also an end product of the starch degradation pathway. The starch content constantly rose through the light period, as it was previously described in many other studies (e.g. (Lu, Gehan, & Sharkey, 2005; Pal et al., 2013)), but reached a plateau in the end of the

day (**Figure 21**), which was also observed for long day conditions before (Nägele et al., 2010; Sulpice et al., 2014). The diagonal Jacobian entries $\delta\, f(sta)/\, \delta\, sta$, constantly decreased during the day indicating a shrinking influence of starch level changes on the starch metabolic function. Based on the finding that the amount of starch degrading proteins does not change significantly during the light period (Lu et al., 2005), the decreasing Jacobian entries could be explained with the vice versa increasing concentration, which would result in a saturation of starch degrading proteins. Although, it has been postulated, that starch degradation is most likely not regulated by protein abundance (Hädrich et al., 2012). In general, the values of the diagonal Jacobian entries of starch were very low, indicating a minor role of starch degradation during the light phase, which coincides with numerous previous studies (see e.g. (A. M. Smith, Zeeman, & Smith, 2005)).

8. Conclusion and Outlook

The applied metabolic modelling approach revealed intricate diurnal dynamics of central carbon and nitrogen metabolism. Important parts of amino acid biosynthesis, i.e. central transamination reactions catalysed by enzymes like aspartate aminotransferase or alanine aminotransferase, were identified to be most active in the middle of the day, with a notable lag phase in the first part of the light phase and a decline of activity towards evening. Furthermore, alpha- ketoglutarate and glutamate were identified to occupy a central role of in primary energy metabolism, and an increase in abundance of alpha- ketoglutarate dehydrogenase protein during the light phase could be predicted. The findings of this study could be verified by literature data on corresponding enzyme activities and provided protein abundance measurements, supporting the validity and reliability of the applied covariance based modelling approach.

In general, the interpretation of Jacobian matrix entries significantly facilitates the integration of experimental metabolomics data with metabolic network information when the data were acquired in a time continuous manner. However, by the approximation of Jacobian entries, a steady state is assumed for each individual time point and an extrapolation over a larger time interval is not possible. This is a necessary simplification for this approach, but undoubtedly the transitions between measured time points will not always be linear. Recently, we developed an approach to address the functional dependencies between the points of measurements performed in a diurnal, or other continuous context. A variance weighted regression analysis of the data is performed and used to create time continuous metabolic functions, which are then related to first and second order derivatives of interacting metabolites. This method, like the covariance based inverse calculation presented in this work, relies on a robust biochemical background, but promises to advance interpretation of time continuous data (Nägele, Fürtauer, Nagler, Weiszmann, & Weckwerth, 2016).

9. Appendix – Supplementary Tables and Figures

Table S1 List of all metabolite dependencies and corresponding pathways and enzymes used in Model A.

Jacobian Entry δf[..]/δ[..]		**Associated Pathway**	**Representative Enzyme Reaction (EC Number)**
Function of (δf[..])	**Variable (δ[…])**		
glycine	glycine	photorespiration	2.1.2.1
	glutamate	photorespiration	2.6.1.4
serine	glycine	photorespiration	2.1.2.1
	serine	photorespiration	2.6.1.45
sucrose	sucrose	sucrose export/interconversion/ cleavage	2.4.1.82 3.2.1.26
	galactinol	raffinose biosynthesis	2.4.1.82
	raffinose	raffinose biosynthesis	2.4.1.82
fructose	sucrose	sucrose cleavage	3.2.1.26
	fructose	fructose interconversion/ phosphorylation	2.7.1.4
	raffinose	raffinose cleavage	3.2.1.26
glucose	sucrose	sucrose cleavage	3.2.1.26
	glucose	glucose interconversion/ phosphorylation	2.7.1.1
	melibiose	melibiose cleavage	3.2.1.22
	trehalose	trehalose degradation	3.2.1.28
	maltose	starch degradation	3.2.1.20
raffinose	sucrose	raffinose biosynthesis	2.4.1.82
	raffinose	raffinose interconversion/cleavage	3.2.1.26
	galactinol	raffinose biosynthesis	2.4.1.82
melibiose	raffinose	raffinose cleavage	3.2.1.26
	melibiose	melibiose interconversion/cleavage	3.2.1.22
galactinol	sucrose	raffinose biosynthesis	2.4.1.82
	galactinol	raffinose biosynthesis	2.4.1.82
	myo-inositol	galactinol synthesis	2.4.1.123

Jacobian Entry δf[..]/δ[..]		**Associated Pathway**	**Representative Enzyme Reaction (EC Number)**
Function of (δf[..])	**Variable (δ[…])**		
galactose	galactose	galactose interconversion/ phosphorylation	2.7.1.6
	melibiose	melibiose interconversion/degradation	3.2.1.22
	raffinose	stachyose: degradation	3.2.1.22
myo-inositol	myo-inositol	myo-inositol interconversion/ galactinol synthesis	2.4.1.123
phenylalanine	phenylalanine	phenylalanine interconversion/degradation	2.6.1.57 2.6.1.58
	glutamate	phenylalanine biosynthesis	2.6.1.79 4.2.1.91
tyrosine	tyrosine	tyrosine interconversion/degradation	2.6.1.5
	glutamate	tyrosine biosynthesis	2.6.1.79 1.3.1.78
pyruvate	valine	alanine biosynthesis	2.6.1.66
	pyruvate	pyruvate interconversion/degradation	1.2.4.1 2.6.1.58
	glutamate	valine/leucine/alanine biosynthesis	2.6.1.42 2.6.1.2
valine	pyruvate	valine biosynthesis	2.6.1.42
	valine	valine interconversion/degradation	2.6.1.42
	glutamate	valine biosynthesis	2.6.1.42
leucine	pyruvate	leucine biosynthesis	2.6.1.42
	leucine	leucine interconversion/degradation	2.6.1.42
	glutamate	leucine biosynthesis	2.6.1.42
alanine	pyruvate	alanine biosynthesis	2.6.1.2
	alanine	alanine interconversion/degradation	2.6.1.2
	glutamate	alanine biosynthesis	2.6.1.2
	valine	alanine biosynthesis	2.6.1.66

Jacobian Entry δf[..]/δ[..]		**Associated Pathway**	**Representative Enzyme Reaction (EC Number)**
Function of (δf[..])	**Variable (δ[…])**		
citrate	pyruvate	citrate biosynthesis	1.2.4.1 2.3.3.8
	citrate	citrate interconversion/degradation	4.2.1.3
	oxaloacetate	citrate biosynthesis	1.2.4.1 2.3.3.8
aspartate	aspartate	aspartate interconversion/degradation	6.3.5.4 2.7.2.4 4.2.3.1
	oxaloacetate	aspartate biosynthesis	1.1.1.37 2.6.1.1
	glutamate	aspartate biosynthesis	2.6.1.1
	glutamine	asparagine biosynthesis	6.3.5.4
asparagine	aspartate	asparagine biosynthesis	6.3.5.4
	asparagine	asparagine interconversion/degradation	3.5.1.1
	glutamine	asparagine biosynthesis	6.3.5.4
succinate	alpha-ketoglutarate	succinate biosynthesis	6.2.1.5
	succinate	succinate interconversion/degradation	1.3.5.1
fumarate	succinate	fumarate biosynthesis	1.3.5.1
	fumarate	fumarate interconversion/degradation	4.2.1.2
malate	fumarate	malate biosynthesis	4.2.1.2
	malate	malate interconversion/degradation	1.1.1.37
proline	proline	proline interconversion/degradation	1.5.99.8
	glutamate	proline biosynthesis	2.7.2.11 1.2.1.41 1.5.1.2

Jacobian Entry δf[..]/δ[..]		**Associated Pathway**	**Representative Enzyme Reaction (EC Number)**
Function of (δf[..])	**Variable (δ[…])**		
alpha-ketoglutarate	pyruvate	valine/leucine biosynthesis	2.6.1.42
	glutamate	glutamate interconversion/degradation	2.6.1.2 2.6.1.1 2.6.1.4 2.6.1.79
	citrate	alpha- ketoglutarate biosynthesis	4.2.1.3 1.1.1.41
	oxaloacetate	aspartate biosynthesis	2.6.1.1
	alpha-ketoglutarate	alpha- ketoglutarate interconversion/degradation	1.4.1.13 1.4.1.2 6.2.1.5
glutamate	pyruvate	valine/leucine/alanine biosynthesis	2.6.1.42 2.6.1.2
	aspartate	asparagine biosynthesis	6.3.5.4
	oxaloacetate	aspartate biosynthesis	2.6.1.1
	glutamate	glutamate interconversion/degradation	2.6.1.42 2.6.1.2 6.3.5.4 2.6.1.1 2.6.1.4 2.6.1.79 1.3.1.78 2.7.2.11 4.1.1.19 3.5.3.11
	glutamine	tryptophan/asparagine biosynthesis	6.3.5.4 4.1.3.27
	alpha-ketoglutarate	glutamate biosynthesis	1.4.1.13 1.4.1.2

Jacobian Entry δf[..]/δ[..]		**Associated Pathway**	**Representative Enzyme Reaction (EC Number)**
Function of (δf[..])	**Variable (δ[…])**		
glutamine	aspartate	asparagine biosynthesis	6.3.5.4
	glutamate	glutamine biosynthesis	6.3.1.2
	glutamine	glutamine interconversion/degradation	4.1.3.27 6.3.5.4 3.5.1.2
oxaloacetate	glutamate	aspartate biosynthesis	2.6.1.1
	malate	TCA-cycle	1.1.1.37
	oxaloacetate	TCA-cycle	1.1.1.37 2.3.3.1 2.3.3.8
ascorbate	myo-inositol	UDP-α-d-glucuronate biosynthesis	1.13.99.1
	ascorbate	ascorbate interconversion/degradation	1.11.1.11
maltose	starch	starch degradation	3.2.1.1
	maltose	maltose interconversion/degradation	3.2.1.20 5.4.99.16
trehalose	trehalose	trehalose interconversion/degradation	3.2.1.28
starch	starch	starch degradation	3.2.1.1
lysine	glutamate	L-lysine biosynthesis	2.6.1.83
	aspartate	L-lysine biosynthesis	2.7.2.4
	pyruvate	L-lysine biosynthesis	4.3.3.7
isoleucine	pyruvate	isoleucine biosynthesis	2.6.1.42
	isoleucine	isoleucine biosynthesis	2.2.1.6

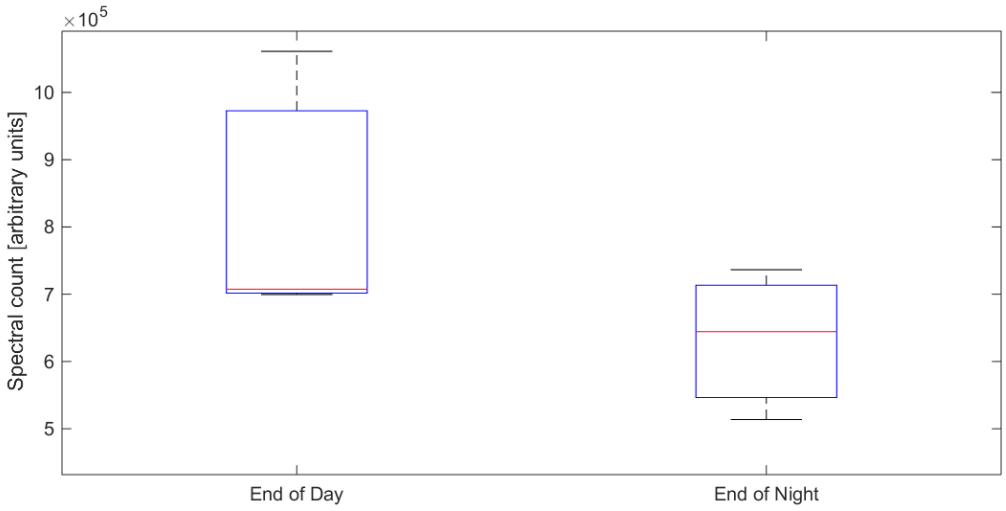

Figure S1 Amount of alpha- ketoglutarate dehydrogenase protein at the end of the day and the end of the night – data provided by Ella Nukarinen (personal notice).

Table S2 Ranking of metabolites in the large, high confidence network, according to their maximum diagonal Jacobian entry.

	06:00	10:00	14:00	18:00	22:00
alpha-ketoglutarate	1.88E+05	2.32E+06	3.14E+06	4.72E+03	1.72E+04
glucose	4.14E+04	2.24E+04	4.32E+02	1.29E-03	2.38E+00
glutamate	6.28E+03	2.01E+04	9.80E+02	2.60E-01	1.63E+01
leucine	4.86E-06	1.09E-07	8.07E-09	5.39E-08	5.95E-09
lysine	1.60E-07	1.86E-08	1.53E-06	1.96E-09	1.49E-09
galactose	3.10E-07	1.10E-06	4.29E-07	7.71E-09	1.15E-08
glycine	2.32E-07	2.69E-08	6.39E-10	3.15E-09	9.88E-10
asparagine	1.61E-07	3.88E-08	5.02E-08	3.10E-08	1.69E-08
galactinol	1.47E-07	7.45E-08	2.23E-08	3.95E-10	3.75E-10
maltose	4.19E-08	8.29E-08	1.90E-08	3.08E-08	2.50E-09
tyrosine	6.59E-08	4.03E-10	1.97E-08	5.66E-10	1.46E-10
glutamine	1.49E-08	5.32E-10	1.02E-09	3.99E-10	8.98E-10
phenylalanine	8.66E-09	1.12E-08	5.47E-11	3.51E-10	2.42E-10
valine	1.07E-08	1.08E-08	6.52E-10	3.49E-10	5.62E-10
fumarate	0	3.64E-10	0	1.00E-08	1.25E-10
trehalose	7.36E-09	8.45E-09	2.50E-10	1.83E-09	5.85E-09
isoleucine	1.10E-10	2.07E-09	1.58E-10	8.41E-09	5.73E-10
pyruvate	5.65E-09	3.53E-09	1.64E-09	8.60E-10	3.81E-10
aspartate	1.15E-09	6.04E-10	1.30E-09	3.41E-09	4.58E-09
serine	1.44E-09	4.24E-09	1.17E-09	1.49E-09	5.60E-10
fructose	2.03E-10	1.99E-09	2.55E-09	3.81E-09	4.05E-10
ascorbate	4.62E-11	1.04E-10	3.69E-09	1.29E-09	1.05E-10
proline	3.54E-09	3.17E-10	3.24E-10	7.27E-10	1.00E-10
citrate	2.84E-09	8.15E-10	1.60E-09	2.91E-11	4.81E-10

alanine	1.30E-09	2.92E-10	1.47E-09	1.39E-09	2.65E-09
sucrose	1.53E-09	1.86E-10	5.30E-10	1.91E-09	0
oxaloacetate	1.37E-09	1.65E-10	7.83E-10	5.95E-11	6.64E-11
malate	5.69E-10	5.86E-12	2.41E-11	9.59E-10	1.53E-10
myo-inositol	9.27E-10	1.14E-10	0	1.45E-11	2.82E-11
melibiose	2.19E-10	3.28E-11	4.57E-10	3.17E-11	3.63E-13
succinate	3.19E-10	1.20E-10	4.22E-10	2.31E-12	2.88E-12
starch	9.93E-12	9.31E-13	6.45E-12	0	0

Table S3 Ranking of all metabolite interactions of the large, primary metabolism network, according to the maximum Jacobian entries,

	06:00	**10:00**	**14:00**	**18:00**	**22:00**
δf(glu)/ δ(kga)	1.41E+07	1.17E+06	1.95E+06	2.44E+00	2.27E+02
δf(glu)/ δ(oxa)	1.30E+07	3.51E+05	1.28E+06	4.81E-01	9.92E+01
δf(glu)/ δ(pyr)	9.83E+06	6.87E+05	9.44E+03	1.81E+01	9.54E+02
δf(kga)/ δ(pyr)	1.93E+05	4.54E+05	3.79E+06	3.70E+02	9.48E+02
δf(glu)/ δ(ala)	3.46E+06	7.46E+05	7.87E+05	3.22E-01	5.72E+01
δf(kga)/ δ(kga)	1.88E+05	2.32E+06	3.14E+06	4.72E+03	1.72E+04
δf(glc)/ δ(tre)	2.41E+06	3.97E+05	7.59E+04	3.83E-01	9.16E+01
δf(kga)/ δ(oxa)	1.42E+05	1.49E+06	1.98E+06	1.77E+03	1.97E+04
δf(glc)/ δ(mel)	1.43E+06	2.17E+05	1.08E+05	9.23E-01	1.74E+02
δf(glu)/ δ(asp)	1.15E+06	4.82E+05	1.73E+05	1.82E+00	2.17E+02
δf(glu)/ δ(gln)	7.75E+05	9.45E+04	3.07E+04	6.85E-01	5.67E+01
δf(kga)/ δ(cit)	1.15E+04	8.33E+04	5.08E+05	2.83E+01	6.68E+02
δf(glc)/ δ(mlt)	4.76E+05	4.98E+05	9.75E+03	4.70E-02	3.67E+01
δf(kga)/ δ(glu)	1.06E+03	4.10E+02	1.76E+05	4.96E+00	5.13E+01
δf(glc)/ δ(glc)	4.14E+04	2.24E+04	4.32E+02	1.29E-03	2.38E+00
δf(glc)/ δ(suc)	2.92E+04	1.13E+04	7.10E+02	3.27E-04	1.93E-01
δf(glu)/ δ(glu)	6.28E+03	2.01E+04	9.80E+02	2.60E-01	1.63E+01
δf(leu)/ δ(leu)	4.86E-06	1.09E-07	8.07E-09	5.39E-08	5.95E-09
δf(lys)/ δ(lys)	1.60E-07	1.86E-08	1.53E-06	1.96E-09	1.49E-09
δf(gal)/ δ(gal)	3.10E-07	1.10E-06	4.29E-07	7.71E-09	1.15E-08
δf(leu)/ δ(pyr)	9.45E-07	5.27E-08	2.80E-08	3.16E-09	2.38E-09
δf(gol)/ δ(gal)	5.70E-07	1.34E-07	3.04E-07	3.47E-09	3.98E-10
δf(gal)/ δ(mel)	1.48E-07	4.35E-07	2.30E-07	2.01E-08	7.76E-10
δf(gly)/ δ(gly)	2.32E-07	2.69E-08	6.39E-10	3.15E-09	9.88E-10
δf(asp)/ δ(asp)	1.61E-07	3.88E-08	5.02E-08	3.10E-08	1.69E-08
δf(asp)/ δ(oxa)	7.88E-09	6.61E-09	1.51E-07	8.59E-10	4.60E-09
δf(gol)/ δ(gol)	1.47E-07	7.45E-08	2.23E-08	3.95E-10	3.75E-10
δf(asp)/ δ(asp)	9.93E-09	4.49E-09	6.85E-09	8.44E-08	1.12E-09
δf(lys)/ δ(asp)	8.41E-09	1.22E-09	8.37E-08	1.13E-08	1.26E-10
δf(mlt)/ δ(mlt)	4.19E-08	8.29E-08	1.90E-08	3.08E-08	2.50E-09
δf(suc)/ δ(gol)	4.94E-09	1.40E-08	2.63E-09	7.50E-08	3.90E-09
δf(tye)/ δ(tye)	6.59E-08	4.03E-10	1.97E-08	5.66E-10	1.46E-10
δf(asp)/ δ(gln)	5.46E-09	5.69E-10	1.37E-09	5.95E-08	1.45E-09

δf(mal)/ δ(oxa)	4.89E-08	4.59E-10	2.18E-08	7.11E-09	6.98E-10
δf(cit)/ δ(oxa)	4.09E-08	1.79E-09	4.62E-09	6.20E-10	1.94E-09
δf(lys)/ δ(pyr)	3.94E-08	3.02E-10	4.03E-08	1.13E-08	1.05E-10
δf(raf)/ δ(gol)	1.30E-09	2.42E-11	9.04E-11	3.66E-08	3.53E-09
δf(ser)/ δ(gly)	3.57E-08	2.20E-09	1.21E-08	1.78E-08	3.72E-09
δf(fum)/ δ(scc)	3.22E-09	4.97E-09	1.50E-09	2.65E-08	2.47E-09
δf(leu)/ δ(glu)	2.48E-08	9.69E-10	4.66E-10	6.35E-11	2.29E-12
δf(ala)/ δ(pyr)	1.79E-09	2.70E-09	2.46E-08	6.77E-09	2.77E-09
δf(gol)/ δ(suc)	2.36E-08	1.65E-12	5.21E-09	2.61E-09	2.75E-11
δf(gol)/ δ(myo)	2.24E-08	5.94E-09	1.12E-08	6.10E-09	3.47E-10
δf(raf)/ δ(raf)	1.17E-09	-5.12E-10	-1.07E-08	-2.63E-07	1.78E-08
δf(gln)/ δ(asp)	5.88E-09	3.23E-10	1.52E-10	1.74E-08	1.69E-08
δf(scc)/ δ(kga)	1.69E-08	5.48E-09	2.32E-09	3.07E-11	1.99E-09
δf(fru)/ δ(raf)	2.12E-10	1.70E-10	9.41E-09	1.63E-08	2.20E-09
δf(cit)/ δ(pyr)	1.63E-08	1.22E-09	4.33E-09	1.09E-09	1.09E-10
δf(lys)/ δ(glu)	2.43E-10	7.92E-11	1.57E-08	6.93E-10	5.42E-12
δf(gln)/ δ(gln)	1.49E-08	5.32E-10	1.02E-09	3.99E-10	8.98E-10
δf(gal)/ δ(raf)	3.70E-09	1.02E-08	1.41E-08	1.02E-09	7.49E-11
δf(phe)/ δ(phe)	8.66E-09	1.12E-08	5.47E-11	3.51E-10	2.42E-10
δf(val)/ δ(val)	1.07E-08	1.08E-08	6.52E-10	3.49E-10	5.62E-10
δf(pyr)/ δ(val)	8.46E-09	1.04E-08	2.10E-09	3.46E-10	1.25E-09
δf(fum)/ δ(fum)	0	3.64E-10	0	1.00E-08	1.25E-10
δf(val)/ δ(pyr)	7.38E-09	3.16E-09	9.35E-09	2.10E-09	5.97E-11
δf(tre)/ δ(tre)	7.36E-09	8.45E-09	2.50E-10	1.83E-09	5.85E-09
δf(ile)/ δ(ile)	1.10E-10	2.07E-09	1.58E-10	8.41E-09	5.73E-10
δf(oxa)/ δ(mal)	4.52E-10	6.93E-11	0	8.23E-09	3.83E-09
δf(ile)/ δ(pyr)	3.59E-09	1.55E-09	7.28E-09	1.06E-09	2.68E-10
δf(ala)/ δ(val)	6.12E-10	8.20E-10	1.30E-09	7.04E-09	3.20E-09
δf(asp)/ δ(gln)	4.10E-10	8.48E-10	1.15E-10	6.64E-09	4.75E-11
δf(pyr)/ δ(pyr)	5.65E-09	3.53E-09	1.64E-09	8.60E-10	3.81E-10
δf(fum)/ δ(mal)	3.14E-09	4.49E-09	7.49E-11	5.48E-09	0
δf(phe)/ δ(gln)	4.74E-10	2.72E-10	3.06E-10	4.81E-09	3.23E-13
δf(asp)/ δ(asp)	1.15E-09	6.04E-10	1.30E-09	3.41E-09	4.58E-09
δf(ser)/ δ(ser)	1.44E-09	4.24E-09	1.17E-09	1.49E-09	5.60E-10
δf(mal)/ δ(fum)	2.95E-10	6.81E-12	0	4.19E-09	4.94E-11
δf(fru)/ δ(fru)	2.03E-10	1.99E-09	2.55E-09	3.81E-09	4.05E-10
δf(oxa)/ δ(glu)	0	2.54E-10	2.16E-10	3.77E-09	3.73E-09
δf(asc)/ δ(asc)	4.62E-11	1.04E-10	3.69E-09	1.29E-09	1.05E-10
δf(pro)/ δ(pro)	3.54E-09	3.17E-10	3.24E-10	7.27E-10	1.00E-10
δf(ser)/ δ(gln)	2.17E-10	3.28E-09	1.81E-10	2.50E-09	3.24E-10
δf(suc)/ δ(raf)	2.08E-09	3.24E-09	5.13E-10	2.96E-09	2.79E-11
δf(asc)/ δ(myo)	2.21E-09	2.00E-10	5.36E-10	3.10E-09	5.39E-10
δf(cit)/ δ(cit)	2.84E-09	8.15E-10	1.60E-09	2.91E-11	4.81E-10
δf(ala)/ δ(ala)	1.30E-09	2.92E-10	1.47E-09	1.39E-09	2.65E-09
δf(raf)/ δ(suc)	1.45E-09	4.65E-13	3.58E-11	2.45E-09	4.89E-11
δf(pro)/ δ(glu)	1.94E-09	2.34E-10	6.32E-10	1.57E-10	1.37E-10
δf(suc)/ δ(suc)	1.53E-09	1.86E-10	5.30E-10	1.91E-09	0

δf(gln)/ δ(glu)	1.87E-09	1.18E-10	9.74E-10	1.57E-09	1.08E-09
δf(asp)/ δ(glu)	1.75E-10	1.99E-10	1.77E-09	6.88E-10	4.47E-10
δf(mel)/ δ(raf)	5.44E-10	7.73E-11	1.60E-09	1.85E-11	0
δf(gly)/ δ(glu)	1.53E-09	1.42E-09	1.04E-09	6.62E-12	5.90E-11
δf(val)/ δ(glu)	2.22E-10	1.26E-10	1.52E-09	6.65E-13	1.01E-13
δf(pyr)/ δ(glu)	3.70E-10	1.50E-10	1.51E-09	5.06E-12	4.87E-11
δf(oxa)/ δ(oxa)	1.37E-09	1.65E-10	7.83E-10	5.95E-11	6.64E-11
δf(mlt)/ δ(sta)	1.19E-09	4.85E-12	9.95E-12	1.63E-11	3.68E-12
δf(phe)/ δ(glu)	7.11E-11	6.47E-10	1.02E-10	1.04E-09	6.22E-13
δf(mal)/ δ(mal)	5.69E-10	5.86E-12	2.41E-11	9.59E-10	1.53E-10
δf(myo)/ δ(myo)	9.27E-10	1.14E-10	0	1.45E-11	2.82E-11
δf(fru)/ δ(suc)	5.47E-10	4.68E-12	6.75E-10	8.80E-10	4.52E-10
δf(mel)/ δ(mel)	2.19E-10	3.28E-11	4.57E-10	3.17E-11	3.63E-13
δf(tye)/ δ(glu)	0	0	4.56E-10	0	3.54E-12
δf(scc)/ δ(scc)	3.19E-10	1.20E-10	4.22E-10	2.31E-12	2.88E-12
δf(sta)/ δ(sta)	9.93E-12	9.31E-13	6.45E-12	0	0

Table S4 Interaction matrix of large, high confidence network, Functions are represented in columns, dependent on metabolite levels in rows (continued on next page)

	raf	ser	tre	gln	asc	asp	mlt	gly	leu	gol	gal	kga	scc	ile	cit	asp	fru	fum	ala	lys	myn	val	pyr	phe	glc	suc	pro	tyr	mel	glu	mal	oxa	ac	sta
raf	1	0	0	0	0	0	0	0	0	0	1	0	0	0	0	0	1	0	0	0	0	0	0	0	0	1	0	0	1	0	0	0	0	0
ser	0	1	0	0	0	0	0	0	0	0	0	0	0	0	0	0	0	0	0	0	0	0	0	0	0	0	0	0	0	0	0	0	0	0
tre	0	0	1	0	0	0	0	0	0	0	0	0	0	0	0	0	0	0	0	0	0	0	0	0	1	0	0	0	0	0	0	0	0	0
gln	0	1	0	1	0	1	0	0	0	0	0	0	0	0	0	1	0	0	0	0	0	0	0	1	0	0	0	0	0	1	0	0	0	0
asc	0	0	0	0	1	0	0	0	0	0	0	0	0	0	0	0	0	0	0	0	0	0	0	0	0	0	0	0	0	0	0	0	0	0
asp	0	0	0	0	0	1	0	0	0	0	0	0	0	0	0	0	0	0	0	0	0	0	0	0	0	0	0	0	0	0	0	0	0	0
mlt	0	0	0	0	0	0	1	0	0	0	0	0	0	0	0	0	0	0	0	0	0	0	0	0	1	0	0	0	0	0	0	0	0	0
gly	0	1	0	0	0	0	0	1	0	0	0	0	0	0	0	0	0	0	0	0	0	0	0	0	0	0	0	0	0	0	0	0	0	0
leu	0	0	0	0	0	0	0	0	1	0	0	0	0	0	0	0	0	0	0	0	0	0	0	0	0	0	0	0	0	0	0	0	0	0
gol	1	0	0	0	0	0	0	0	0	1	0	0	0	0	0	0	0	0	0	0	0	0	0	0	0	1	0	0	0	0	0	0	0	0
gal	0	0	0	0	0	0	0	0	0	1	1	0	0	0	0	0	0	0	0	0	0	0	0	0	0	0	0	0	0	0	0	0	0	0
kga	0	0	0	0	0	0	0	0	0	0	0	1	1	0	0	0	0	0	0	0	0	0	0	0	0	0	0	0	0	1	0	0	0	0
scc	0	0	0	0	0	0	0	0	0	0	0	0	1	0	0	0	0	1	0	0	0	0	0	0	0	0	0	0	0	0	0	0	0	0
ile	0	0	0	0	0	0	0	0	0	0	0	0	0	1	0	0	0	0	0	0	0	0	0	0	0	0	0	0	0	0	0	0	0	0
cit	0	0	0	0	0	0	0	0	0	0	0	1	0	0	1	0	0	0	0	0	0	0	0	0	0	0	0	0	0	0	0	0	0	0
asp	0	0	0	1	0	1	0	0	0	0	0	0	0	0	0	1	0	0	0	1	0	0	0	0	0	0	0	0	0	1	0	0	0	0
fru	0	0	0	0	0	0	0	0	0	0	0	0	0	0	0	0	1	0	0	0	0	0	0	0	0	0	0	0	0	0	0	0	1	0
fum	0	0	0	0	0	0	0	0	0	0	0	0	0	0	0	0	0	1	0	0	0	0	0	0	0	0	0	0	0	0	1	0	0	0
ala	0	0	0	0	0	0	0	0	0	0	0	0	0	0	0	0	0	0	1	0	0	0	0	0	0	0	0	0	0	0	0	0	0	0
lys	0	0	0	0	0	0	0	0	0	0	0	0	0	0	0	0	0	0	0	1	0	0	0	0	0	0	0	0	0	0	0	0	0	0
myn	0	0	0	0	1	0	0	0	0	1	0	0	0	0	0	0	0	0	0	0	1	0	0	0	0	0	0	0	0	0	0	0	0	0
val	0	0	0	0	0	0	0	0	0	0	0	0	0	0	0	0	0	0	0	0	0	1	1	0	0	0	0	0	0	0	0	0	0	0
pyr	0	0	0	0	0	0	0	0	1	0	0	1	0	1	1	0	0	0	1	1	0	1	1	0	0	0	0	0	0	1	0	0	0	0

Table S4 (continued)

	raf	ser	tre	gln	asc	asp	mlt	gly	leu	gol	gal	kga	scc	ile	cit	asp	fru	fum	ala	lys	myn	val	pyr	phe	glc	suc	pro	tyr	mel	glu	mal	oxa	ac	sta
phe	0	0	0	0	0	0	0	0	0	0	0	0	0	0	0	0	0	0	0	0	0	0	0	1	0	0	0	0	0	0	0	0	0	0
glc	0	0	0	0	0	0	0	0	0	0	0	0	0	0	0	0	0	0	0	0	0	0	0	0	1	0	0	0	0	0	0	0	1	0
suc	1	0	0	0	0	0	0	0	0	1	0	0	0	0	0	0	1	0	0	0	0	0	0	0	1	1	0	0	0	0	0	0	0	0
pro	0	0	0	0	0	0	0	0	0	0	0	0	0	0	0	0	0	0	0	0	0	0	0	0	0	0	1	0	0	0	0	0	0	0
tyr	0	0	0	0	0	0	0	0	0	0	0	0	0	0	0	0	0	0	0	0	0	0	0	0	0	0	0	1	0	0	0	0	0	0
mel	0	0	0	0	0	0	0	0	0	0	1	0	0	0	0	0	0	0	0	0	0	0	0	0	1	0	0	0	1	0	0	0	0	0
glu	0	0	0	1	0	0	0	1	1	0	0	1	0	0	0	1	0	0	1	1	0	1	1	1	0	0	1	1	0	1	0	1	0	0
mal	0	0	0	0	0	0	0	0	0	0	0	0	0	0	0	0	0	1	0	0	0	0	0	0	0	0	0	0	0	0	1	1	0	0
oxa	0	0	0	0	0	0	0	0	0	0	0	1	0	0	1	1	0	0	0	0	0	0	0	0	0	0	0	0	0	0	1	1	0	0
ac	0	0	1	0	0	0	0	1	0	0	0	0	0	0	0	0	0	0	0	0	1	0	1	0	0	1	0	0	0	0	0	0	1	1
sta	0	0	0	0	0	0	1	0	0	0	0	0	0	0	0	0	0	0	0	0	0	0	0	0	0	0	0	0	0	0	0	0	0	1

Table S5 Abbreviations used in **Table S4**

raffinose	raf	galactinol	gol	alanine	ala	tyrosine	tyr
serine	ser	galactose	gal	lysine	lys	melibiose	mel
trehalose	tre	alpha-ketoglutarate	kga	myo-inositol	myn	glutamate	glu
glutamine	gln	succinate	scc	valine	val	malate	mal
ascorbate	asc	isoleucine	ile	pyruvate	pyr	oxaloacetate	oxa
asparagine	asp	citrate	cit	phenylalanine	phe	Activated Compounds	ac
maltose	mlt	aspartate	asp	glucose	glc	Starch	sta
glycine	gly	fructose	fru	sucrose	suc		
leucine	leu	fumarate	fum	proline	pro		

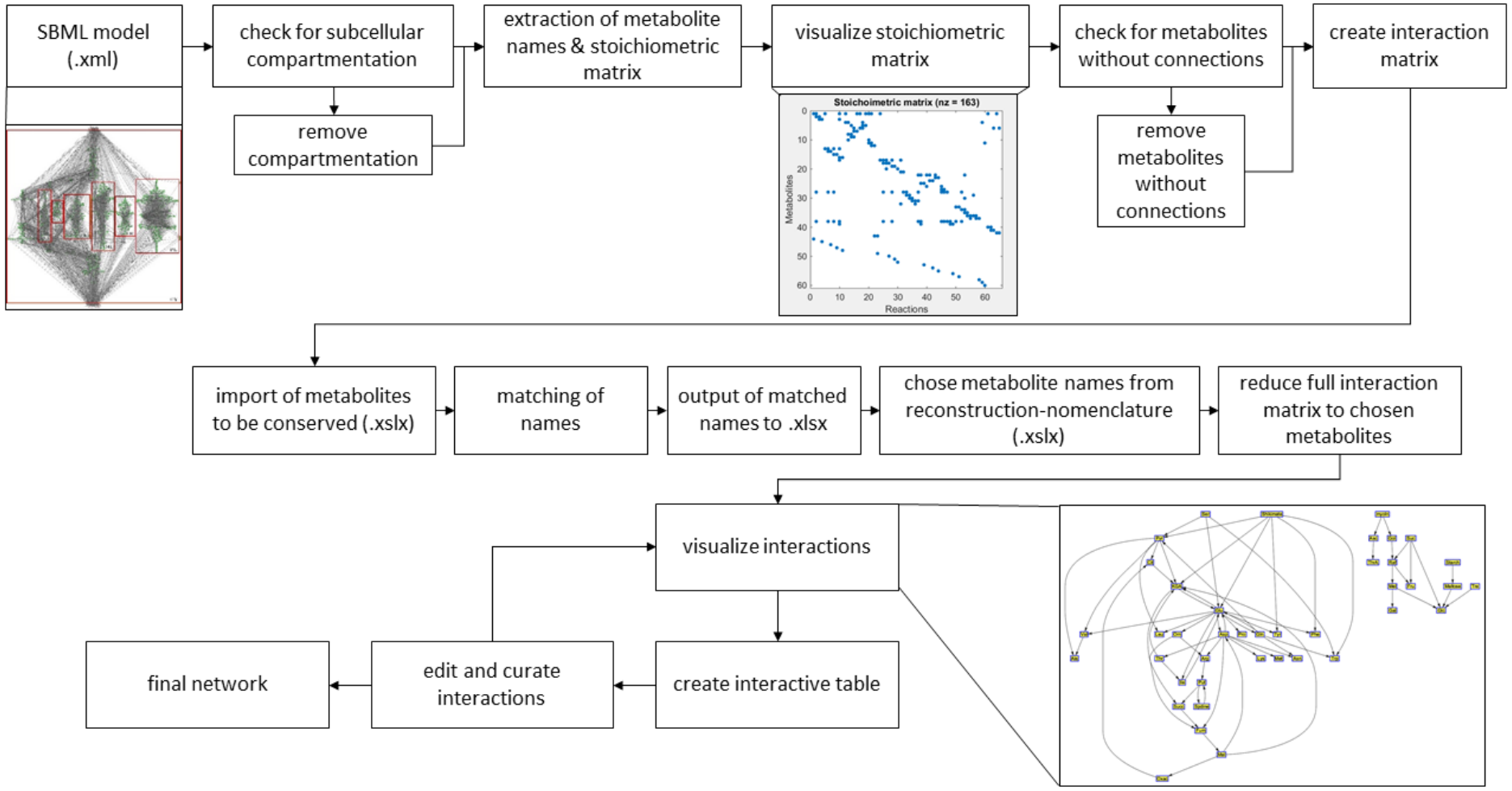

Figure S2 Visualisation of the workflow for network reduction

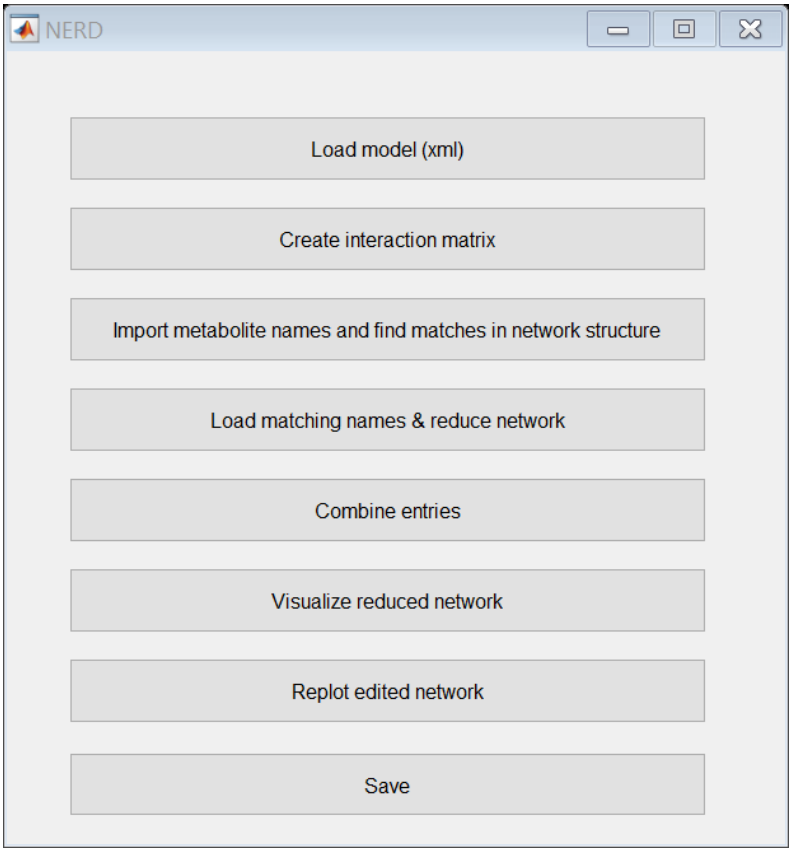

Figure S3 GUI of the presented MATLAB workflow for the extraction of core metabolic networks from genome scale metabolic reconstructions. NERD – Network Reduction Device

10. Literature

Bauer, A., Urquhart, A. A., & Joy, K. W. (1977). Amino Acid metabolism of pea leaves: labeling studies on utilization of amides. *Plant Physiology*, *59*(5), 920–924. http://doi.org/10.1104/pp.59.5.920

Berg, J. M., Stryer, L., & Tymoczko, J. L. (2015). *Stryer Biochemie*.

Blaesing, O. E., Gibon, Y., Günther, M., Höhne, M., Morcuende, R., Osuna, D., … Ho, M. (2005). Sugars and circadian regulation make major contributions to the global regulation of diurnal gene expression in Arabidopsis. *The Plant Cell*, *17*(12), 3257–3281. http://doi.org/10.1105/tpc.105.035261

Caspi, R., Altman, T., Billington, R., Dreher, K., Foerster, H., Fulcher, C. A., … Karp, P. D. (2014). The MetaCyc database of metabolic pathways and enzymes and the BioCyc collection of Pathway/Genome Databases. *Nucleic Acids Research*, *42*(D1), D459–D471. http://doi.org/10.1093/nar/gkt1103

Covington, M. F., Maloof, J. N., Straume, M., Kay, S. A., & Harmer, S. L. (2008). Global transcriptome analysis reveals circadian regulation of key pathways in plant growth and development. *Genome Biology*, *9*(8), R130. http://doi.org/10.1186/gb-2008-9-8-r130

de Oliveira Dal'Molin, C. G., Quek, L.-E., Palfreyman, R. W., Brumbley, S. M., & Nielsen, L. K. (2010). AraGEM, a genome-scale reconstruction of the primary metabolic network in Arabidopsis. *Plant Physiology*, *152*(2), 579–89. http://doi.org/10.1104/pp.109.148817

Dodd, A. N., Salathia, N., Hall, A., Kévei, E., Tóth, R., Nagy, F., … Webb, A. a R. (2005). Plant circadian clocks increase photosynthesis, growth, survival, and competitive advantage. *Science (New York, N.Y.)*, *309*(5734), 630–633. http://doi.org/10.1126/science.1115581

Doerfler, H., Lyon, D., Nägele, T., Sun, X., Fragner, L., Hadacek, F., … Weckwerth, W. (2013). Granger causality in integrated GC-MS and LC-MS metabolomics data reveals the interface of primary and secondary metabolism. *Metabolomics : Official Journal of the Metabolomic Society*, *9*(3), 564–574. http://doi.org/10.1007/s11306-012-0470-0

Funahashi, A., Matsuoka, Y., Jouraku, A., Kitano, H., & Kikuchi, N. (2006). CELLDESIGNER: A MODELING TOOL FOR BIOCHEMICAL NETWORKS Akira. In *Proceedings of the 2006 Winter Simulation Conference* (Vol. 1707, p. 1712). http://doi.org/10.1017/CBO9781107415324.004

Gibon, Y., Blaesing, O. E., Hannemann, J., Carillo, P., Höhne, M., Hendriks, J. H. M., … Stitt, M. (2004). A Robot-based platform to measure multiple enzyme activities in Arabidopsis using a set of cycling assays: comparison of changes of enzyme activities and transcript levels during diurnal cycles and in prolonged darkness. *The Plant Cell*, *16*(December), 3304–3325. http://doi.org/10.1105/tpc.104.025973

Gibon, Y., Blaesing, O. E., Palacios-Rojas, N., Pankovic, D., Hendriks, J. H. M., Fisahn, J., … Stitt, M. (2004). Adjustment of diurnal starch turnover to short days: Depletion of sugar during the night leads to a temporary inhibition of carbohydrate utilization, accumulation of sugars and post-translational activation of ADP-glucose pyrophosphorylase in the followin. *Plant Journal*, *39*(6), 847–862. http://doi.org/10.1111/j.1365-313X.2004.02173.x

Gutenkunst, R. N., Waterfall, J. J., Casey, F. P., Brown, K. S., Myers, C. R., & Sethna, J. P. (2007). Universally sloppy parameter sensitivities in systems biology models. *PLoS Computational Biology*, *3*(10), 1871–1878. http://doi.org/10.1371/journal.pcbi.0030189

Hädrich, N., Hendriks, J. H. M., Kötting, O., Arrivault, S., Feil, R., Zeeman, S. C., … Lunn, J. E. (2012). Mutagenesis of cysteine 81 prevents dimerization of the APS1 subunit of ADP-glucose pyrophosphorylase and alters diurnal starch turnover in Arabidopsis thaliana leaves. *The Plant Journal*, *70*(2), 231–242. http://doi.org/10.1111/j.1365-313X.2011.04860.x

Harmer, S. L. (2009). The circadian system in higher plants. *Annual Review of Plant Biology*, *60*(1), 357–77. http://doi.org/10.1146/annurev.arplant.043008.092054

Hoffmann, M. H. (2002). Biogeography of Arabidopsis thaliana (L .). *Journal of Biogeography*, *29*, 125–134. http://doi.org/10.1046/j.1365-2699.2002.00647.x

Hoops, S., Gauges, R., Lee, C., Pahle, J., Simus, N., Singhal, M., … Kummer, U. (2006). COPASI - A COmplex PAthway SImulator. *Bioinformatics*, *22*(24), 3067–3074.

http://doi.org/10.1093/bioinformatics/btl485

Hsu, C. H., & Lo, Y. M. (2003). Characterization of xanthan gum biosynthesis in a centrifugal, packed-bed reactor using metabolic flux analysis. *Process Biochemistry*, *38*(11), 1617–1625. http://doi.org/10.1016/S0032-9592(03)00054-2

Hucka, M., Finney, A., Sauro, H. M., Bolouri, H., Doyle, J. C., Kitano, H., … Wang, J. (2003). The systems biology markup language (SBML): A medium for representation and exchange of biochemical network models. *Bioinformatics*, *19*(4), 524–531. http://doi.org/10.1093/bioinformatics/btg015

Juty, N., Ali, R., Glont, M., Keating, S., Rodriguez, N., Swat, M., … Chelliah, V. (2015). BioModels: Content, Features, Functionality, and Use. *CPT: Pharmacometrics & Systems Pharmacology*, *4*(2), 55–68. http://doi.org/10.1002/psp4.3

Kadereit, J. W., Kost, B., & Sonnewald, U. (2014). *Strasburger Lehrbuch der Pflanzenwissenschaften*.

Koornneef, M., Alonso-Blanco, C., & Vreugdenhil, D. (2004). Naturally Occurring Genetic Variation in Arabidopsis Thaliana. *Annual Review of Plant Biology*, *55*(1), 141–172. http://doi.org/10.1146/annurev.arplant.55.031903.141605

Laibach, F. (1943). Arabidopsis thaliana (L.) Heynh. als Objekt für genetische und entwicklungsphysiologische Untersuchungen. *Bot. Archiv*.

Lu, Y., Gehan, J. P., & Sharkey, T. D. (2005). Daylength and circadian effects on starch degradation and maltose metabolism. *Plant Physiology*, *138*(4), 2280–2291. http://doi.org/10.1104/pp.105.061903

Mairan, J. de. (1729). Observation botanique. *Hist. Acad. Roy. Sci*.

Mancuso, S., & Shabala, S. (2007). *Rhythms in Plants: Phenomenology, Mechanisms, and Adaptive Significance*. Springer Science & Business Media.

Mani, K. M., Lefebvre, C., Wang, K., Lim, W. K., Basso, K., Dalla-Favera, R., & Califano, A. (2008). A systems biology approach to prediction of oncogenes and molecular perturbation targets in B-cell lymphomas. *Molecular Systems Biology*, *4*(1), 169. http://doi.org/10.1038/msb.2008.2

Matt, P., Schurr, U., Klein, D., Krapp, A., & Stitt, M. (1998). Growth of tobacco in short-day conditions leads to high starch, low sugars, altered diurnal changes in the Nia transcript and low nitrate reductase activity, and inhibition of amino acid synthesis. *Planta*, *207*(1), 27–41. http://doi.org/10.1007/s004250050452

Meadows, A. L., Karnik, R., Lam, H., Forestell, S., & Snedecor, B. (2010). Application of dynamic flux balance analysis to an industrial Escherichia coli fermentation. *Metabolic Engineering*, *12*(2), 150–160. http://doi.org/10.1016/j.ymben.2009.07.006

Merlet, B., Paulhe, N., Vinson, F., Frainay, C., Chazalviel, M., Poupin, N., … Jourdan, F. (2016). A Computational Solution to Automatically Map Metabolite Libraries in the Context of Genome Scale Metabolic Networks. *Frontiers in Molecular Biosciences*, *3*(February), 1–12. http://doi.org/10.3389/fmolb.2016.00002

Minton, A. P. (2001). The Influence of Macromolecular Crowding and Macromolecular Confinement on Biochemical Reactions in Physiological Media. *Journal of Biological Chemistry*, *276*(14), 10577–10580. http://doi.org/10.1074/jbc.R100005200

Mintz-Oron, S., Meir, S., Malitsky, S., Ruppin, E., Aharoni, A., & Shlomi, T. (2012). Reconstruction of Arabidopsis metabolic network models accounting for subcellular compartmentalization and tissue-specificity. *Proceedings of the National Academy of Sciences of the United States of America*, *109*(1), 339–44. http://doi.org/10.1073/pnas.1100358109

Mockler, T. C., Michael, T. P., Priest, H. D., Shen, R., Sullivan, C. M., Givan, S. A., … Chory, J. (2007). The diurnal project: Diurnal and circadian expression profiling, model-based pattern matching, and promoter analysis. In *Cold Spring Harbor Symposia on Quantitative Biology* (Vol. 72, pp. 353–363). http://doi.org/10.1101/sqb.2007.72.006

Moore, B., Zhou, L., Rolland, F., Hall, Q., Cheng, W.-H., Liu, Y.-X., … Sheen, J. (2003). Role of the Arabidopsis Glucose Sensor HXK1 in Nutrient, Light, and Hormonal Signaling. *Science*, *300*(5617), 332–336. http://doi.org/10.1126/science.1080585

Nägele, T. (2014). Linking metabolomics data to underlying metabolic regulation. *Frontiers in Molecular Biosciences*, *1*(November), 1–6. http://doi.org/10.3389/fmolb.2014.00022

Nägele, T., Fürtauer, L., Nagler, M., Weiszmann, J., & Weckwerth, W. (2016). A Strategy for Functional

Interpretation of Metabolomic Time Series Data in Context of Metabolic Network Information . *Frontiers in Molecular Biosciences* .

Nägele, T., Henkel, S., Hörmiller, I., Sauter, T., Sawodny, O., Ederer, M., & Heyer, A. G. (2010). Mathematical modeling of the central carbohydrate metabolism in Arabidopsis reveals a substantial regulatory influence of vacuolar invertase on whole plant carbon metabolism. *Plant Physiology*, *153*(1), 260–72. http://doi.org/10.1104/pp.110.154443

Nägele, T., Mair, A., Sun, X., Fragner, L., Teige, M., & Weckwerth, W. (2014). Solving the differential biochemical jacobian from metabolomics covariance data. *PLoS ONE*, *9*(4).

Nägele, T., & Weckwerth, W. (2013). A workflow for mathematical modeling of subcellular metabolic pathways in leaf metabolism of Arabidopsis thaliana. *Frontiers in Plant Science*, *4*, 541. http://doi.org/10.3389/fpls.2013.00541

Orth, J. D., Conrad, T. M., Na, J., Lerman, J. A., Nam, H., Feist, A. M., & Palsson, B. Ø. (2011). A comprehensive genome-scale reconstruction of Escherichia coli metabolism. *Molecular Systems Biology*, *7*(1), 535. http://doi.org/10.1038/msb.2011.65

Pal, S. K., Liput, M., Piques, M., Ishihara, H., Obata, T., Martins, M. C. M., … Stitt, M. (2013). Diurnal changes of polysome loading track sucrose content in the rosette of wild-type arabidopsis and the starchless pgm mutant. *Plant Physiology*, *162*(3), 1246–65. http://doi.org/10.1104/pp.112.212258

Pracharoenwattana, I., Zhou, W., Keech, O., Francisco, P. B., Udomchalothorn, T., Tschoep, H., … Smith, S. M. (2010). Arabidopsis has a cytosolic fumarase required for the massive allocation of photosynthate into fumaric acid and for rapid plant growth on high nitrogen. *Plant Journal*, *62*(5), 785–795. http://doi.org/10.1111/j.1365-313X.2010.04189.x

Rolland, F., Baena-Gonzalez, E., & Sheen, J. (2006). Sugar Sensing and Signaling in Plants: Conserved and Novel Mechanisms. *Annual Review of Plant Biology*, *57*(1), 675–709. http://doi.org/10.1146/annurev.arplant.57.032905.105441

Rolland, F., Moore, B., & Sheen, J. (2002). Sugar Sensing and Signaling in Plants. *The Plant Cell*, *14*(Suppl), s185–s205. http://doi.org/10.1105/tpc.010455

Ryu, J. Y., Kim, H. U., & Lee, S. Y. (2015). Reconstruction of genome-scale human metabolic models using omics data. *Integrative Biology : Quantitative Biosciences from Nano to Macro*, *7*(8), 859–68. http://doi.org/10.1039/c5ib00002e

Safer, B., & Williamson, J. R. (1973). Mitochondrial-Cytosolic Interactions in Perfused Rat Heart. *The Journal of Biological Chemistry*, *248*(7), 2570–2597.

Schaber, J., Liebermeister, W., & Klipp, E. (2009). Nested uncertainties in biochemical models. *IET Systems Biology*, *3*(1), 1–9. http://doi.org/10.1049/iet-syb:20070042

Schallau, K., & Junker, B. H. (2010). Simulating Plant Metabolic Pathways with Enzyme-Kinetic Models. *Plant Physiology*, *152*(4), 1763–1771. http://doi.org/10.1104/pp.109.149237

Scheible, W.-R., Krapp, A., & Stitt, M. (2000). Reciprocal diurnal changes of phosphoenolpyruvate carboxylase expression and cytosolic pyruvate kinase, citrate synthase and NADP-isocitrate dehydrogenase expression regulate organic acid metabolism during nitrate assimilation in tobacco leaves. *Plant, Cell and Environment*, *23*(11), 1155–1167. http://doi.org/10.1046/j.1365-3040.2000.00634.x

Schopfer, P., & Brennicke, A. (2010). *Pflanzenphysiologie*.

Smith, A. M., Zeeman, S. C., & Smith, S. M. (2005). Starch Degradation. *Annual Review of Plant Biology*, *56*(1), 73–98. http://doi.org/10.1146/annurev.arplant.56.032604.144257

Smith, S., Fulton, D. C., Chia, T., Thorneycroft, D., Chapple, A., Dunstan, H., … Smith, A. M. (2004). Diurnal changes in the transcriptome encoding enzymes of starch metabolism provide evidence for both transcriptional and posttranscriptional regulation of starch metabolism in Arabidopsis leaves. *Plant Physiology*, *136*(1), 2687–99. http://doi.org/10.1104/pp.104.044347

Steuer, R. (2007). Computational approaches to the topology, stability and dynamics of metabolic networks. *Phytochemistry*, *68*(16-18), 2139–2151. http://doi.org/10.1016/j.phytochem.2007.04.041

Steuer, R., Kurths, J., Fiehn, O., & Weckwerth, W. (2003). Observing and interpreting correlations in metabolomic networks. *Bioinformatics*, *19*(8), 1019–1026.

http://doi.org/10.1093/bioinformatics/btg120

Stitt, M., Müller, C., Matt, P., Gibon, Y., Carillo, P., Morcuende, R., … Krapp, A. (2002). Steps towards an integrated view of nitrogen metabolism. *Journal of Experimental Botany*, *53*(370), 959–970. http://doi.org/10.1093/jexbot/53.370.959

Sulpice, R., Flis, A., Ivakov, A. A., Apelt, F., Krohn, N., Encke, B., … Stitt, M. (2014). Arabidopsis Coordinates the Diurnal Regulation of Carbon Allocation and Growth across a Wide Range of Photoperiods. *Molecular Plant*, *7*(1), 137–155. http://doi.org/10.1093/mp/sst127

Sun, X., & Weckwerth, W. (2012). COVAIN: a toolbox for uni- and multivariate statistics, time-series and correlation network analysis and inverse estimation of the differential Jacobian from metabolomics covariance data. *Metabolomics*, *8*(S1), 81–93. http://doi.org/10.1007/s11306-012-0399-3

Teusink, B., Passarge, J., Reijenga, C. a, Eshalgado, E., van der Weijden, C. C., Schepper, M., … Snoep, J. (2000). Can yeast glycolysis be understood in terms of in vitro kientics of the constitutent enzyme? Testing biochemnistry. *European Journal of Biochemnistry*, *267*(February), 5313–5329.

Thiele, I., & Palsson, B. Ø. (2010). A protocol for generating a high-quality genome-scale metabolic reconstruction. *Nature Protocols*, *5*(1), 93–121. http://doi.org/10.1038/nprot.2009.203

Töpfer, N., Kleessen, S., & Nikoloski, Z. (2015). Integration of metabolomics data into metabolic networks. *Frontiers in Plant Science*, *6*, 49. http://doi.org/10.3389/fpls.2015.00049

Tretter, L., & Adam-Vizi, V. (2005). Alpha-ketoglutarate dehydrogenase: a target and generator of oxidative stress. *Philosophical Transactions of the Royal Society of London. Series B, Biological Sciences*, *360*(1464), 2335–2345. http://doi.org/10.1098/rstb.2005.1764

Van Kampen, N. G. (1992). *Stochastic processes in physics and chemistry* (Vol. 1). Elsevier.

Watson, E., Yilmaz, L. S., & Walhout, A. J. M. (2015). Understanding Metabolic Regulation at a Systems Level: Metabolite Sensing, Mathematical Predictions, and Model Organisms. *Annual Review of Genetics*, *49*(1), 553–575. http://doi.org/10.1146/annurev-genet-112414-055257

Zeeman, S. C., Smith, S. M., & Smith, A. M. (2004). The breakdown of starch in leaves. *New Phytologist*, *163*(2), 247–261. http://doi.org/10.1111/j.1469-8137.2004.01101.x